Earthquakes as point sources

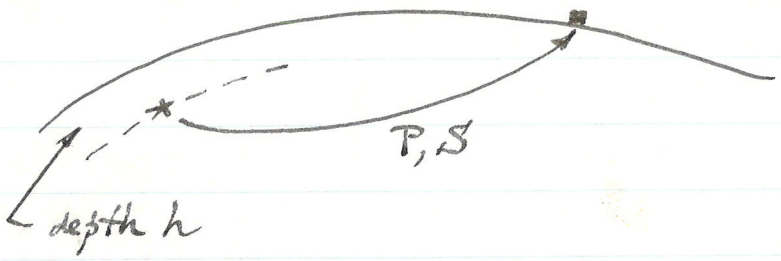

epicenter vs. hypocenter

Location: depth h
lat., long.
origin time

With 4 or more P times from distant stations, least squares fit for location and origin time. This done routinely now by ISC.

Local 'quakes (crustal): measure P and S arrival time

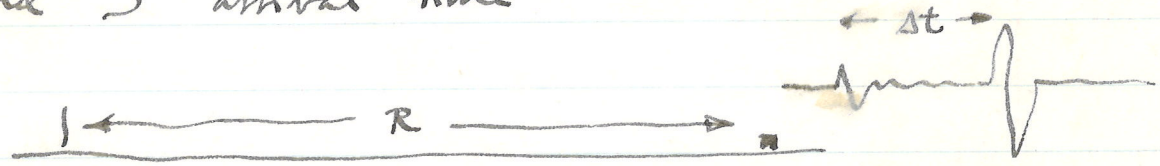

$v_p = 6$ km/s
$v_s = 4$ km/s
} typical crustal velocities

Let $t_p \equiv$ time of P arrival − origin time (unknown) = travel time of P wave

$$R = 6 t_p = 4 (t_p + \Delta t)$$
$$t_p = 2 \Delta t$$

If $\Delta t = 1$ sec, $t_p = 2$ sec, $R = 12$ km

This equivalent to

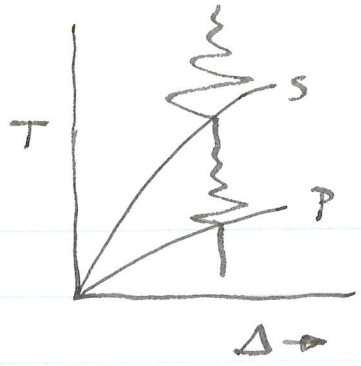

Use several stations and string + circle method to locate

Depth is generally most poorly constrained parameter. For int. to deep-focus teleseismic events, pP is useful here

Local events can be located to within 100's of meters with an extensive local array, important to know if on old faults or not. Crustal velocity inhomogeneities main problem. Different velocities on 2 sides of SA fault caused all events to be routinely mislocated to one side of fault for many years.

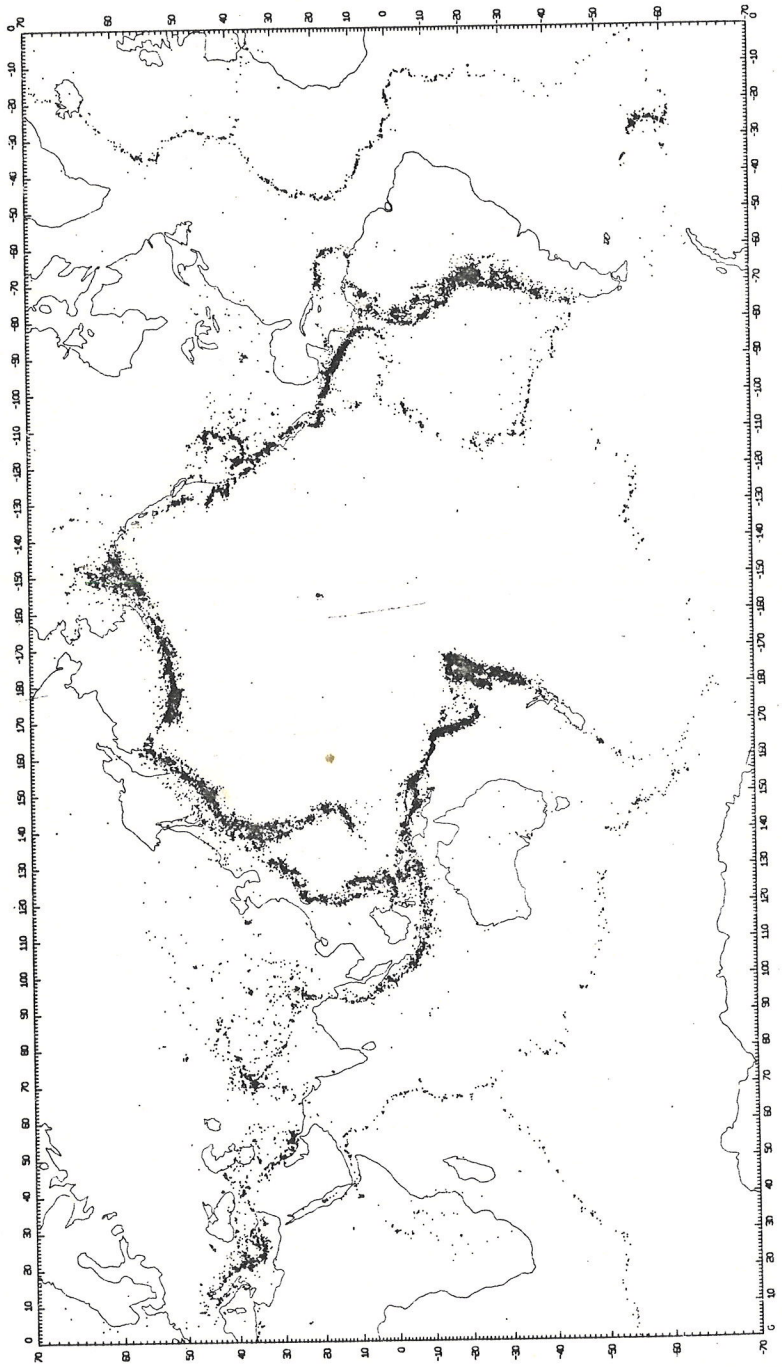

Figure 5.1. Epicenters of 29,000 earthquakes 1961–1967, depths 0–700 km, plotted by Barazangi and Dorman (1969) and reproduced, by permission, from their manuscript.

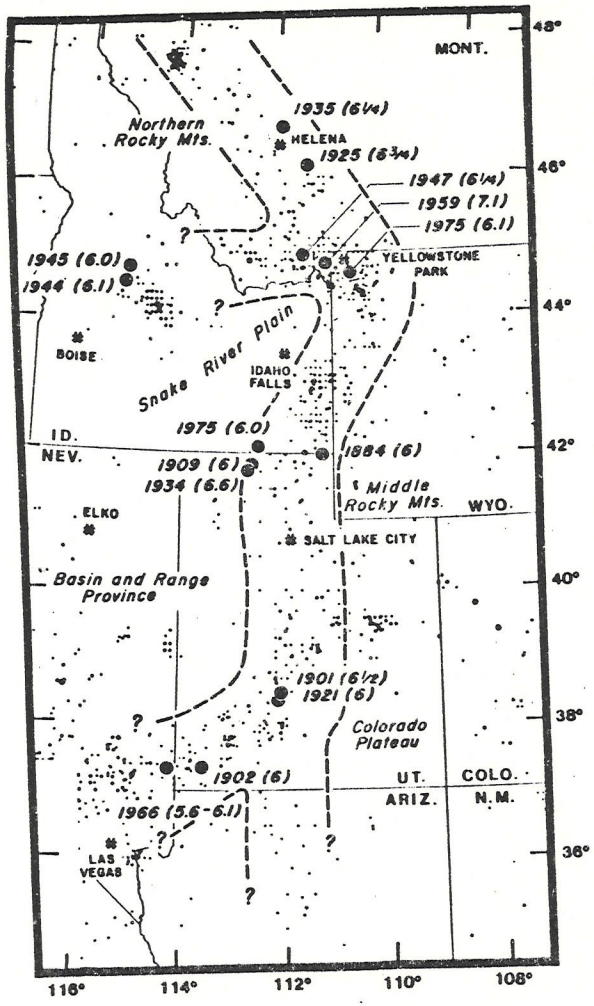

Figure 2a — Index map of Intermountain seismic belt. Epicenters of historical mainshocks ($M \geqslant 6.0$) shown as large circles, NOAA epicenters through 1974 as smaller circles. Schematic dashed outline of seismic belt based on various seismotectonic studies as well as depicted seismicity. Magnitudes (in parentheses) are estimated or measured values of M_L, except values for 1925–1959 (attributed to Pasadena), which are either m_b or M_s. Epicenter of 1966 shock (M_L5.6, m_b6.1) added for reference. (from Arabasz and Smith)

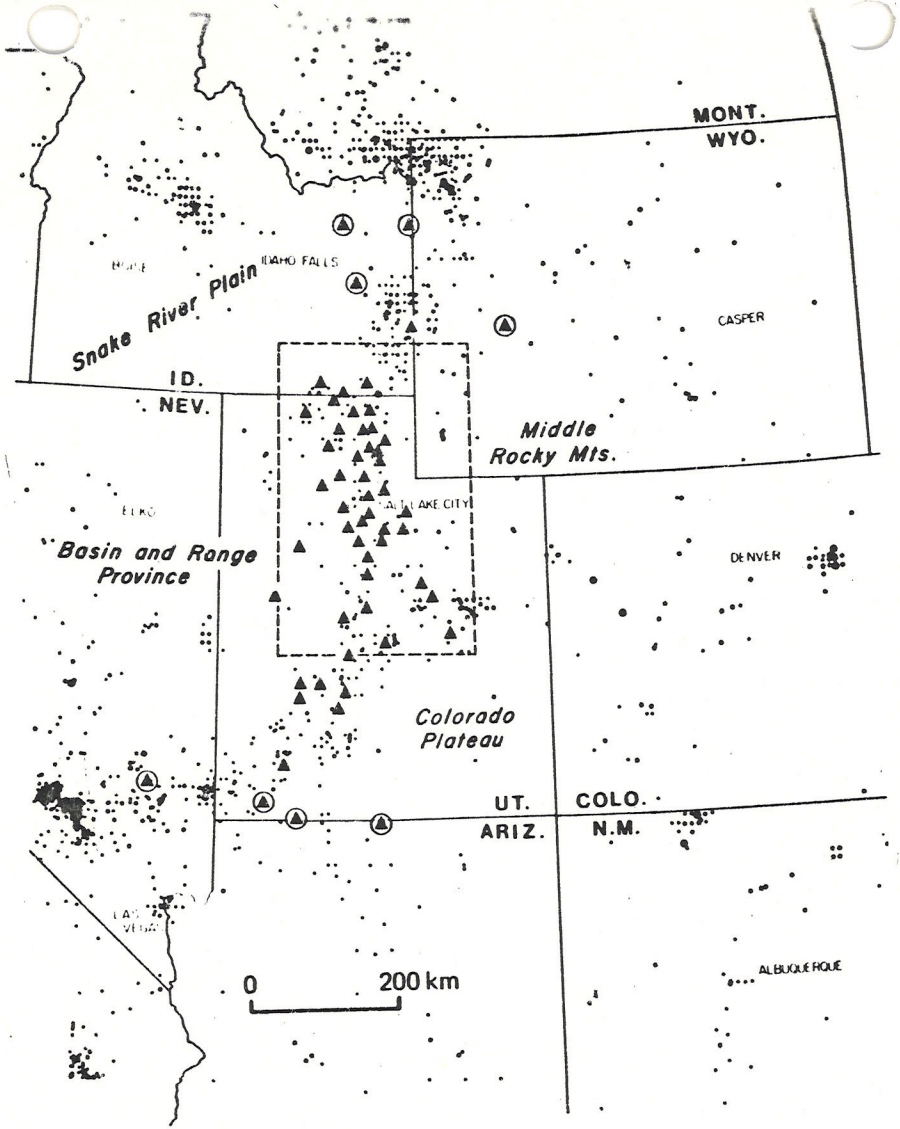

UNIVERSITY OF UTAH SEISMIC NETWORK

Figure 2b — Index map showing seismograph stations (triangles) of the University of Utah telemetered seismic network in relation to regional earthquake epicenters (small circles) of the Intermountain seismic belt. Circumscribed triangles indicate stations owned and operated by other agencies but centrally recorded by the University of Utah. Dashed line outlines Wasatch front study area. (Epicenter map after Smith, 1978)

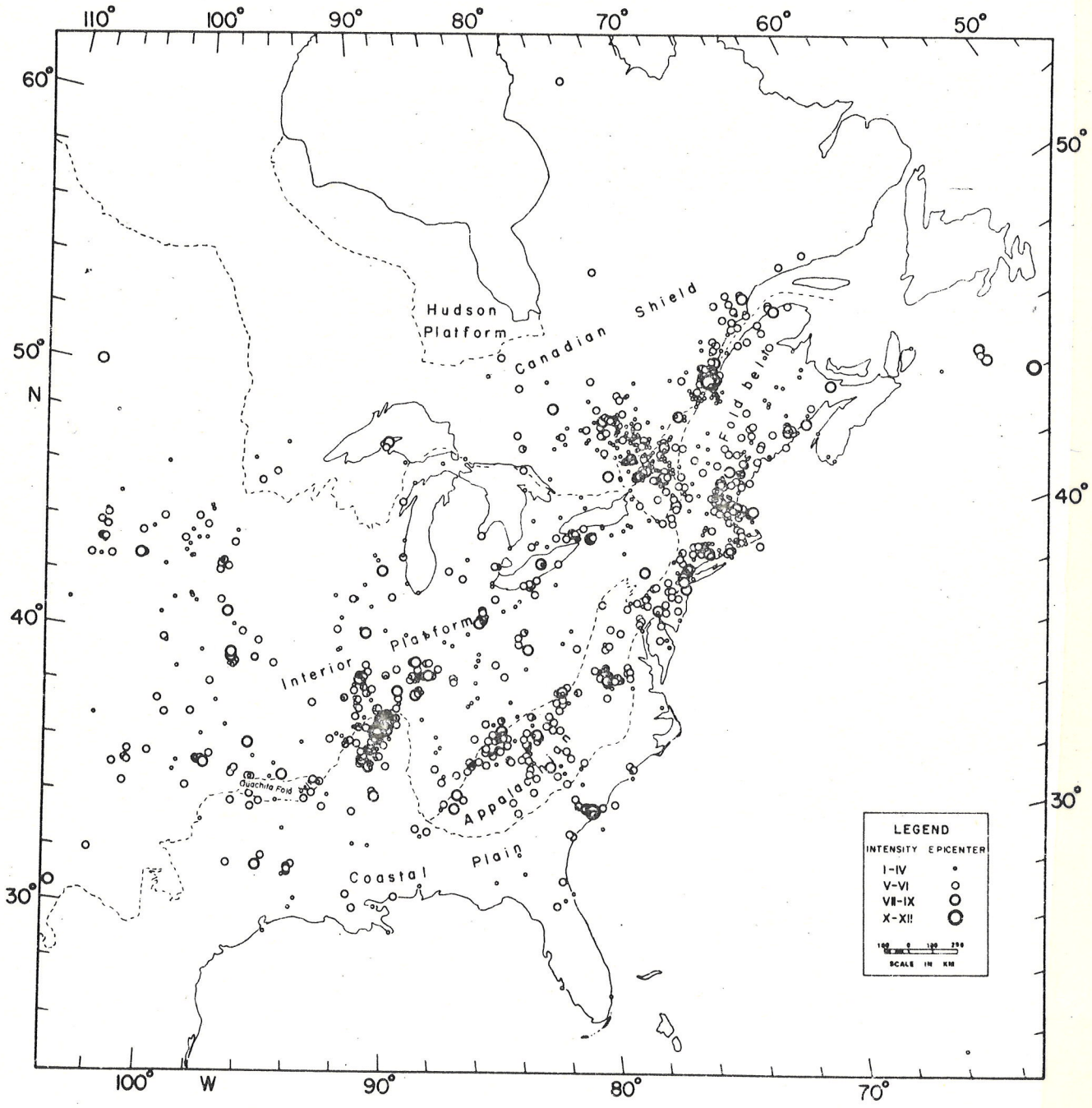

Fig. 14. Distribution of reported earthquakes in eastern North America, 1534–1971, from historical and instrumental data [after *York and Oliver,* 1976]. Note activity along the Appalachian fold belt, the northwest trending zone in New England and southern Quebec, and the northwesterly trend in South Carolina.

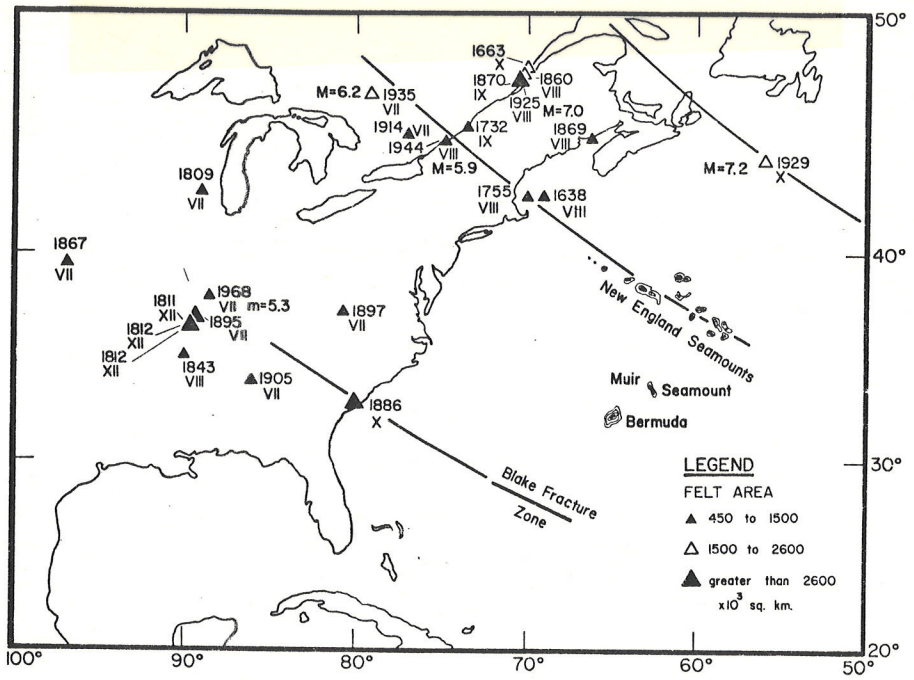

Fig. 12. Historic earthquakes in eastern North America [after *Fletcher et al.*, 1978]. Only earthquakes with felt areas greater than 450,000 km² and intensities of VII or greater are shown. Three small circles (solid lines) were drawn about a single center of rotation for the early opening of the Atlantic Ocean. These three small circles (transform directions) were started at the three major offsets (transform faults) in the magnetic lineation pattern of Mesozoic age in the western Atlantic and extended into eastern North America. Note that several of the larger historic shocks fall close to the small circle passing along the New England (Kelvin) seamount chain.

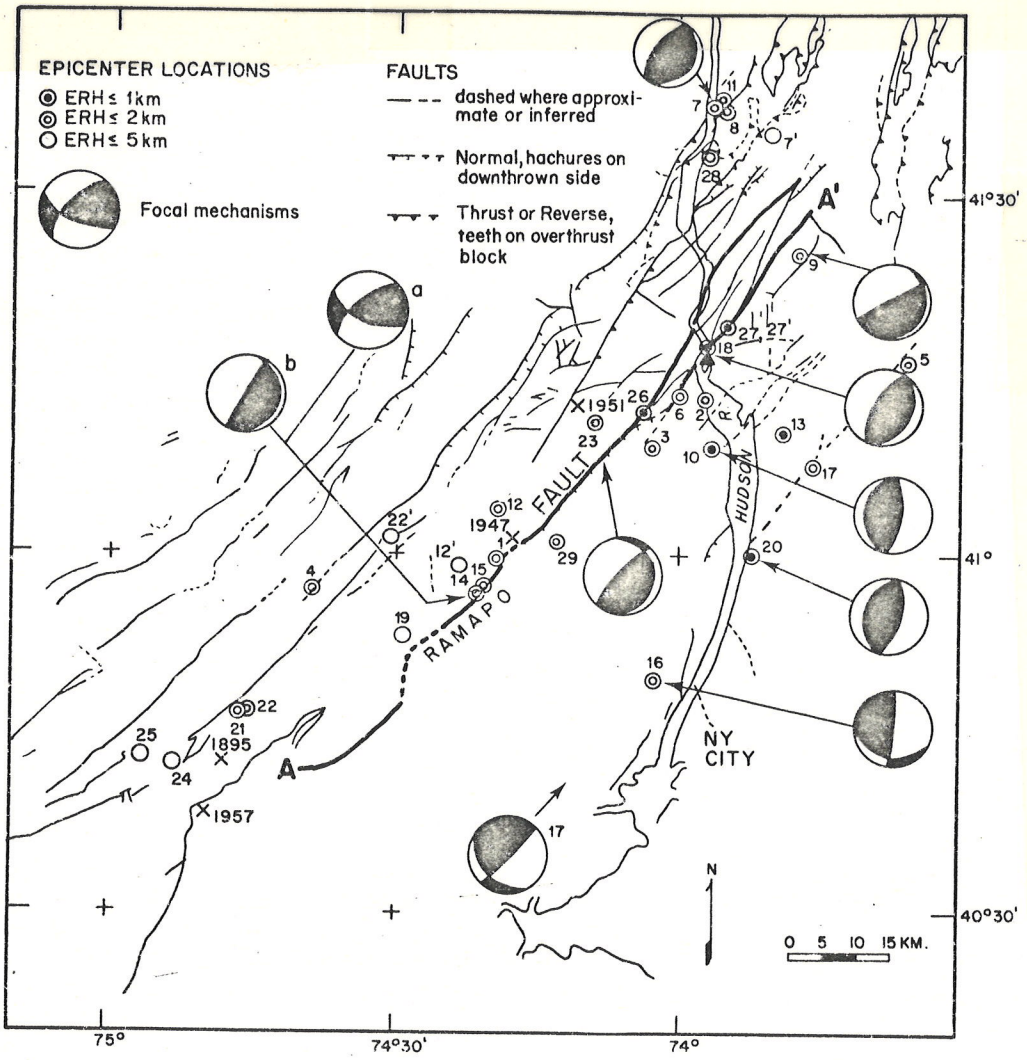

Fig. 22. Fault map of southeastern New York and northern New Jersey showing epicenters (circles) of instrumentally located earthquakes from 1962 to 1977, after *Aggarwal and Sykes* [1978]. Indicated uncertainties (ERH) in epicentral locations represent approximately 2 standard deviations. Focal mechanism solutions (FMS) are upper hemisphere plots; dark area represents the compressional quadrant. Note that for event 14 there are two possible FMS; the data, however, are more consistent with solution b than with solution a. The Ramapo fault and two of its major branches (A-A') are shown by heavy lines. Crosses denote locations for older events near the Ramapo fault. Triangle shows location of nuclear power reactors.

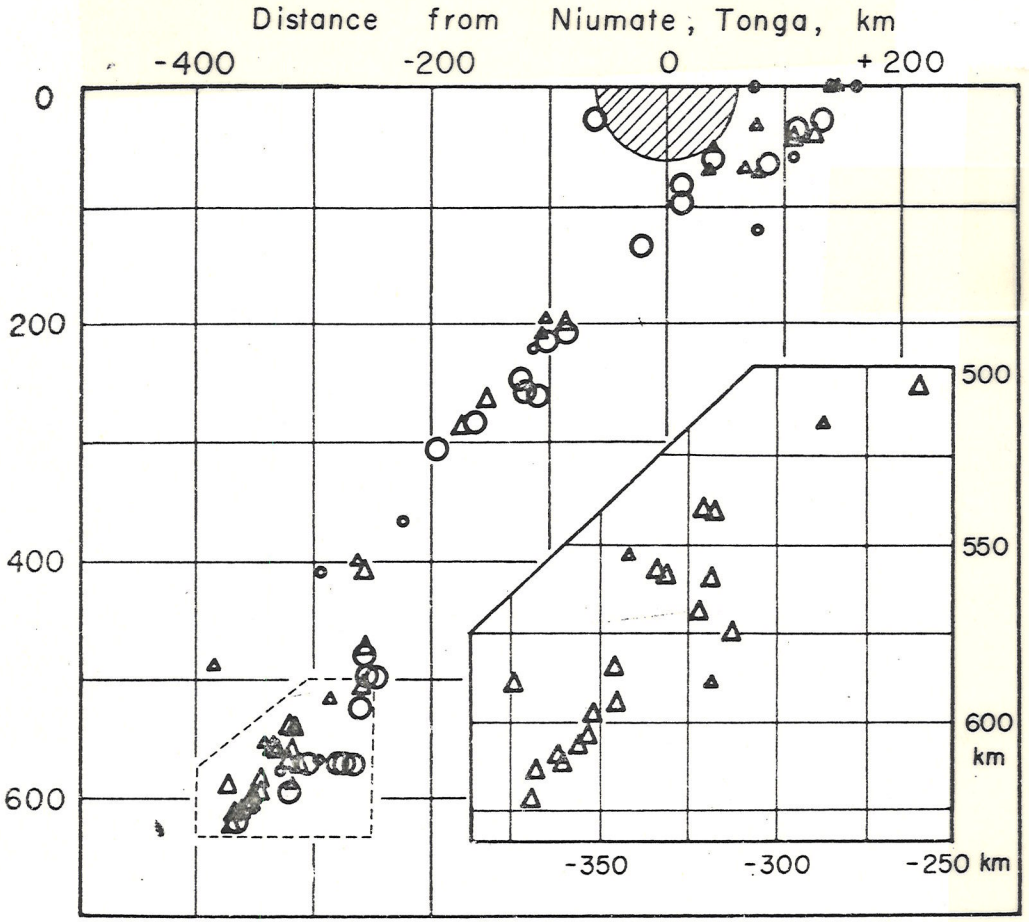

Fig. 9. Vertical section oriented perpendicular to the Tonga arc. Circles represent earthquakes projected from within 0 to 150 km north of the section; triangles correspond to events projected from within 0 to 150 km south of the section. All shocks occurred during 1965 while the Lamont network of stations in Tonga and Fiji was in operation. Locations are based on data from these stations and from more distant stations. No microearthquakes from a sample of 750 events originated from within the hatched region near the station at Niumate, Tonga (i.e., for *S-P* times less than 6.5 sec). A vertical exaggeration of about 13 : 1 was used for the insert showing the topography [after *Raitt et al.*, 1955]; the horizontal and vertical scales are equal in the cross section depicting earthquake locations. Lower insert shows enlargement of southern half of section for depths between 500 and 625 km. Note small thickness (less than ~20 km) of seismic zone for wide range of depths.

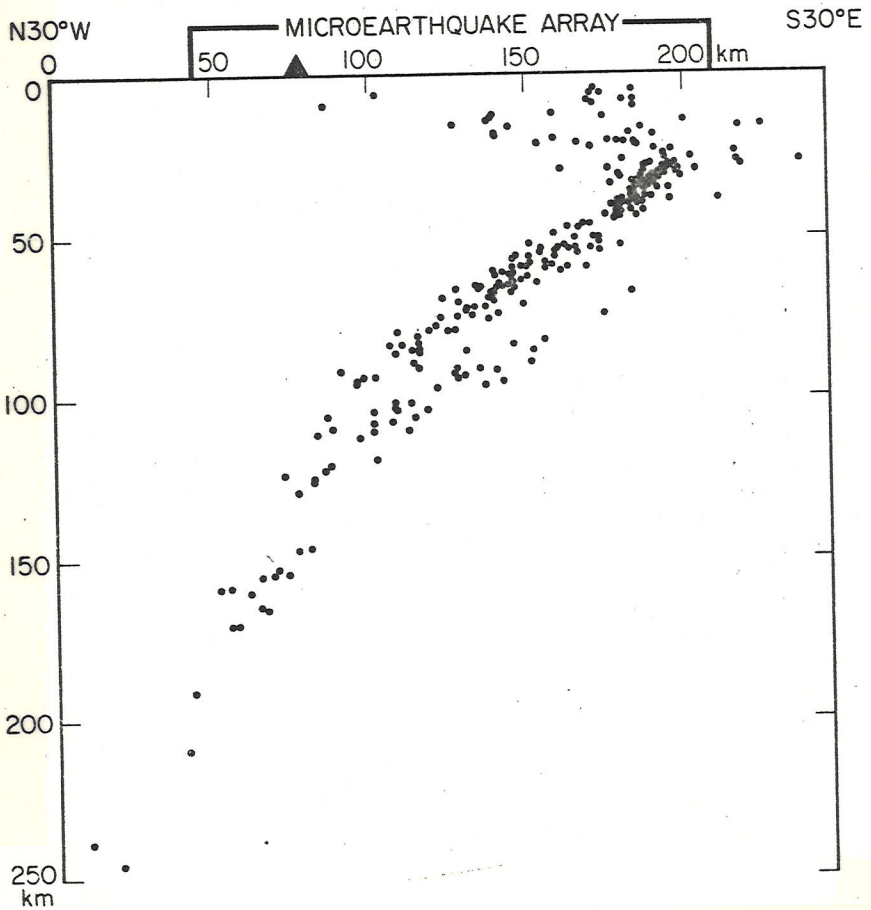

Fig. 3. A depth section of the hypocenters of microearthquakes occurring in the region delimited in Figure 2. The volcanic front is marked by the solid triangle, and vertical and horizontal scales are equal.

Observed quake locations: mostly along plate margins, define plate boundaries.

Also ∃ intraplate 'quakes, thought to be associated in most cases with reactivated old lineaments and basement faults.

Seismicity in East (on passive margin) not well understood. Diffuse seismicity in western states, normal faulting, assoc. with rifting or spreading or extension of Basin + Range province

Only 10% of quakes are deeper than 30 km depth (mostly up in lithosphere which is only part of ⊕ capable of behaving brittly. All int. and deep-focus 'quakes are located in Benioff zones where subducted slabs of cold lithosphere extend down into mantle.

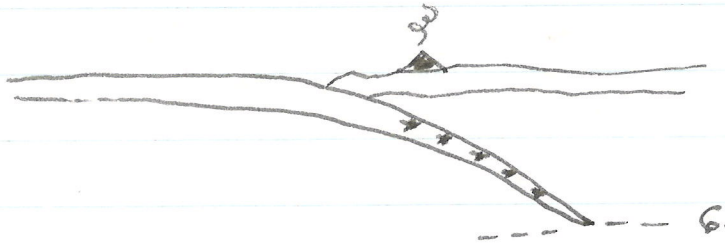

--- 650 km: deepest quakes, now thought that slabs extend below this, just not seismically active.

Earthquake magnitude: an empirical measure of size, introduced by Richter at Caltech in 1930's. Actually 3 different scales in use: local, surface wave and body wave magnitudes.

Local 'quakes in California (original scale)

$$M_L = \log_{10} a + 3 \log_{10} \Delta - 2.92$$

- M_L: local
- $\log_{10} a$: ground ampl. in μm
- $3 \log_{10} \Delta$: corrects for ampl. atten. with distance (empirically); a comb. of both $1/\sqrt{\text{area}}$ and anelastic
- used only for $\Delta \leq 600$ km

Calibrated to give $M = 0$ a maximum 1 μm trace on seismogram (Wood–Anderson: mag. = 2800) at $\Delta = 100$ km.

Surface wave magnitude M_S commonly reported for typical teleseismic event is based on amplitude of ~20 s surface wave

$$M_S = \log_{10} a + 1.7 \log_{10} \Delta + \text{const.}$$

- $\log_{10} a$: 20 s Rayleigh wave ground amplitude
- $1.7 \log_{10} \Delta$: corrects for falloff with distance
- const.: station-dependent (typically ~1.8)

M_S cannot be used for deep-focus events, as they do not excite visible 20 s surface waves.

For these Gutenberg + Richter introduced the body wave magnitude m_b, based on the ground ampl. of 1 s body waves. Again an empirical formula of the type

$$m_b = \log_{10} a + f(\Delta, h)$$

was employed.

In general the mle is $a \sim 10^M$ where a is the ground amplitude at some standardized distance from the source. The magnitude scale is logarithmic.

An empirical relation has been found

$$m_b = 2.5 + 0.63\, M_S$$
$$M_S = 1.59\, m_b - 3.97$$

$m_b = M_S$ at $6\frac{3}{4}$, above this $M_S > m_b$, below $m_b > M_S$

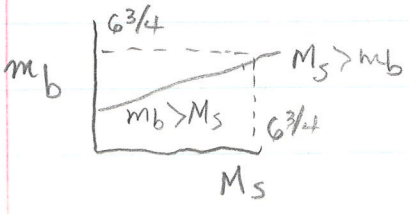

Nuclear explosions give values of M_S consistently lower by about 1 for a given m_b than do 'quakes, which fall along the above empirical curve.

This probably the single most useful discriminant: at same depth h, explosions (more compact) generate smaller surface waves compared to body waves (actually smaller 20 s waves compared to 1 s waves) than 'quakes.

Earthquake energy: energy $\propto$ (ampl)^2
How much total energy is radiated away by source?

Another empirical Gutenberg – Richter formula

$$\log_{10} E = 11.8 + 1.5 M_S \quad \text{ergs}$$

$$E = 10^{11.8 + 1.5 M_S} \quad \text{ergs}$$

Why, if $a \sim 10^M$ does $E \sim 10^{1.5M}$

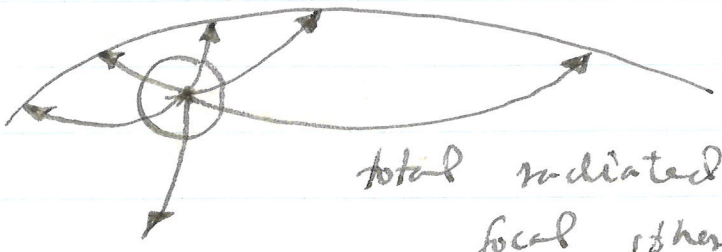

total radiated energy passing focal sphere surrounding source.

M_S	E (ergs)
8.5	$3.6 \cdot 10^{24}$
8.0	$6.3 \cdot 10^{23}$
7.5	$1.1 \cdot 10^{23}$
7.0	$2.0 \cdot 10^{22}$
6.5	$3.6 \cdot 10^{21}$
6.0	$6.3 \cdot 10^{20}$
5.5	$1.1 \cdot 10^{20}$
5.0	$2.0 \cdot 10^{19}$
4.5	$3.6 \cdot 10^{18}$
4.0	$6.3 \cdot 10^{17}$

32 times

1000 times

Numbers of 'quakes: this also investigated by Gutenberg + Richter ('quake statistics)
Found

$$\log_{10} N = a + b(8 - M_S)$$
$$= -0.48 + 0.9(8 - M_S)$$

where

N = # events/yr in the magnitude class $M_S \pm 1$

WWSSN limit →

Magnitude M_S	≥ 8	7.9–7	6.9–6	5.9–5	4.9–4	3.9–3
Frequency N (yr^{-1})	$\lesssim 1$	13	108	800	6200	49K
Energy E (ergs) $\times 10^{23}$	13.7	12.0	1.1	0.8	0.2	0.05
% total energy released in 1 yr	49%	43%	4%	3%	1%	

The occasional very large quake responsible for most of the energy release in quakes. (93% of energy release from $M_S \geq 7$)

Focal mechanism studies: first P-wave motion allows a determination of the nature of faulting associated with an event, e.g. strike-slip fault

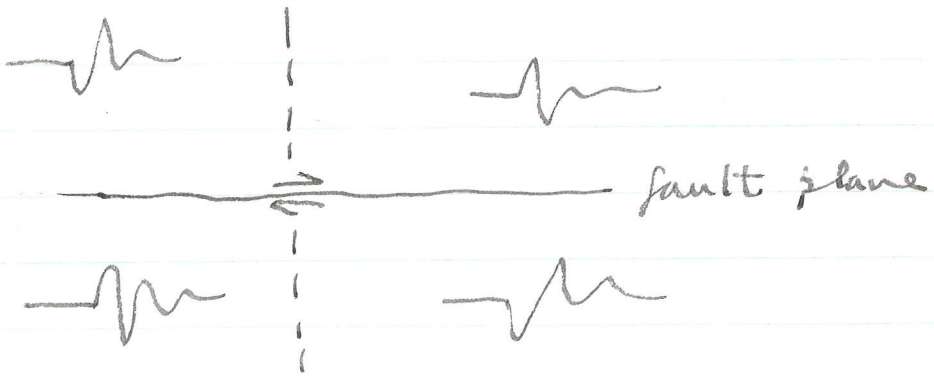

auxiliary plane (dep: normal is direction of slip on fault)

Generalization to 'quakes in a sphere (the ⊕)

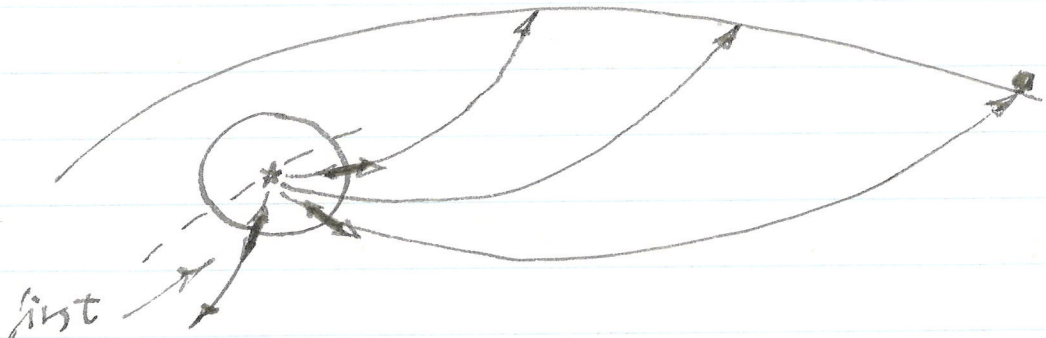

focal sphere : a sphere of unit radius centered on source

Knowing quake location one can trace ray back from a station and determine where it left the focal sphere. Usually one sees only the lower focal hemisphere (rays leaving source going up go to very short Δ's).

Usual procedure (used in our lab exercise) is to plot ups and downs (towards and aways) on an equal area projection (Schmidt or Lambert-Schmidt) of lower focal hemisphere. Equal-area used because it gives station density the "correct" appearance.

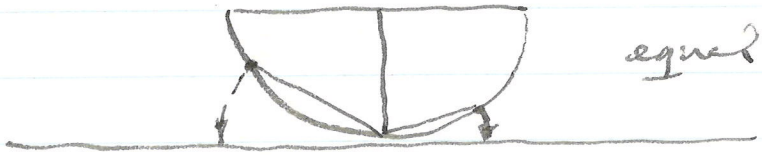

equal – area projection

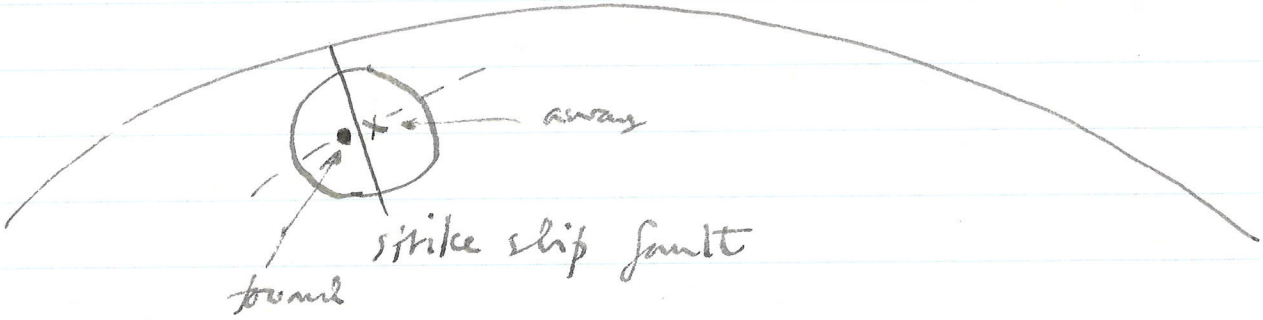

Focal mechanism will look like

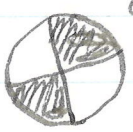

Note: inability to distinguish fault plane from auxiliary plane: this an inherent ambiguity, could be

Must use other geological information, if it is available to decide.

An important application of focal mechanism studies (early 60's – they first became

reliable with advent of LP WWSSN, Sykes' demonstration of correctness of Wilson's transform fault hypothesis

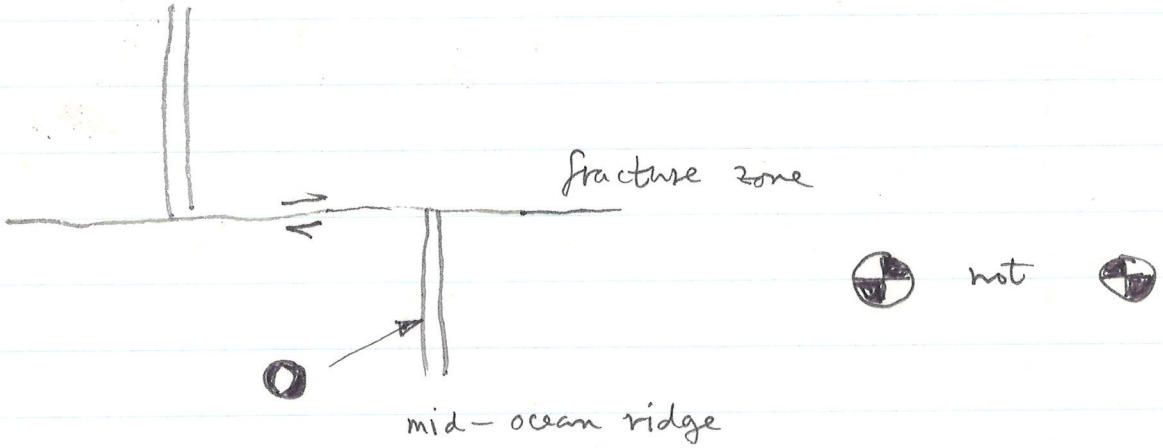

Other types of commonly observed events : or "what do those beach balls mean"?

1. normal faults in extensional environments, e.g. on crests of mid-ocean ridges

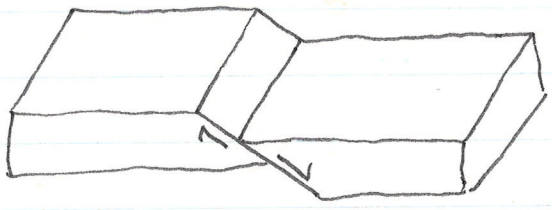

produces 

3. shallow-angle thrust faults : at subduction zones, e.g. 1964 Alaskan 'quake
Stauder + Bollinger

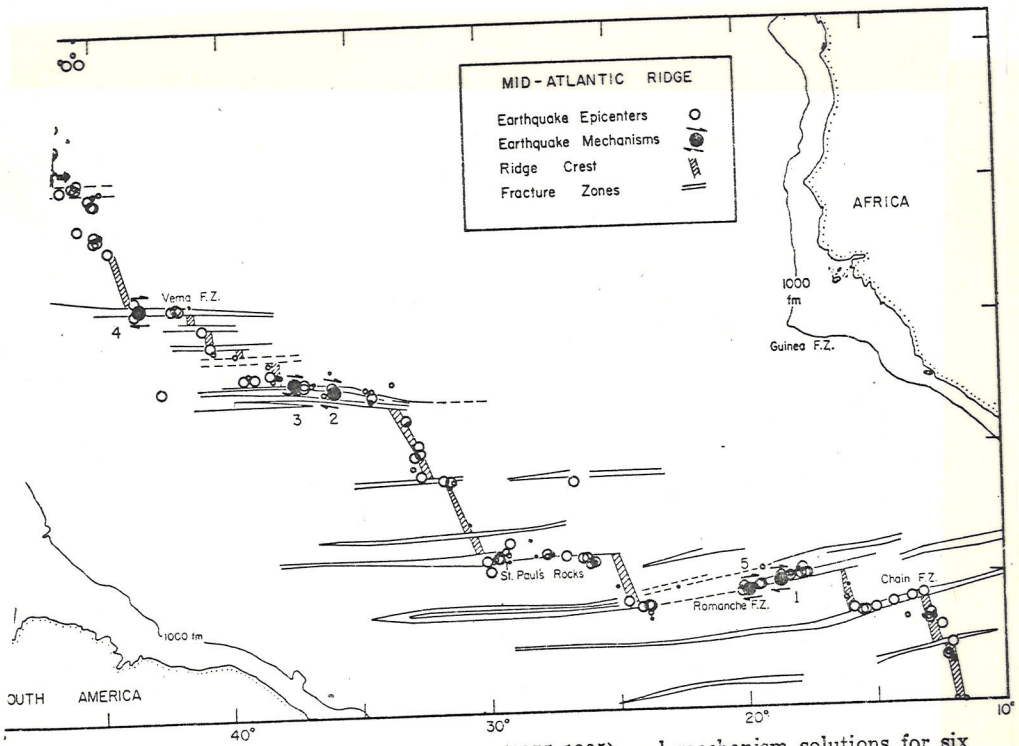

Fig. 2. Relocated epicenters of earthquakes (1955–1965) and mechanism solutions for six earthquakes along part of the Mid-Atlantic ridge. Ridges crests and fracture zones are from *Heezen and Tharp* [1965]. Events 1–5 were characterized by a predominance of right-lateral strike-slip motion on steeply dipping planes that strike approximately east. Event 6 was characterized by a predominance of normal faulting; the axis of maximum tension for this event (heavy arrows) is nearly horizontal and nearly perpendicular to the strike of the ridge. Large circles denote more precise epicentral determinations; smaller circles, poorer determinations; large solid circles denote earthquakes for which the mechanism is illustrated.

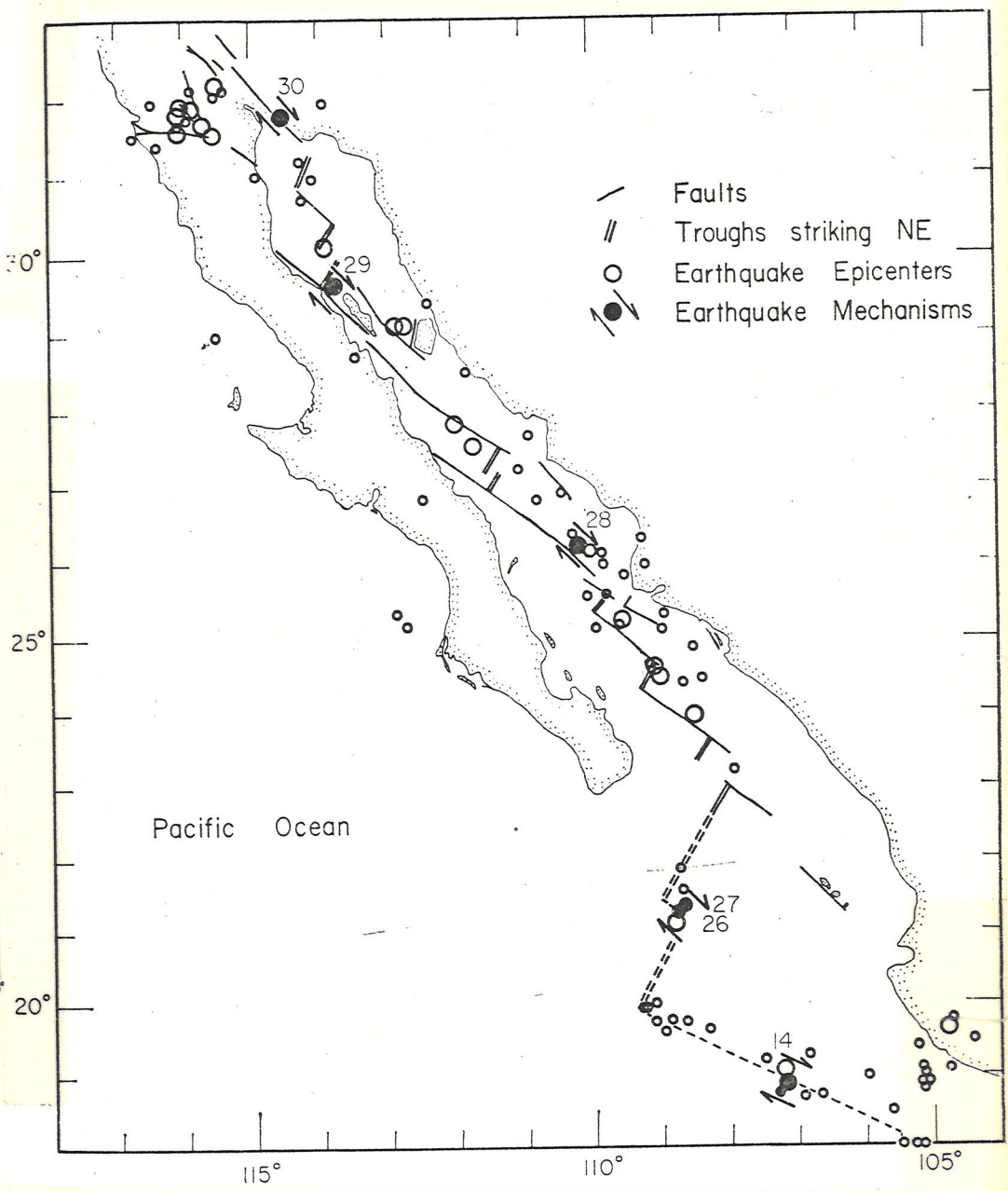

Fig. 6. Structural features of the Gulf of California [after *Sykes*, 1968]. Relocated epicenters of earthquakes for the period 1954 to 1962. Seismicity and focal mechanisms support the hypothesis of spreading by ocean-ridge–transform-fault mechanism.

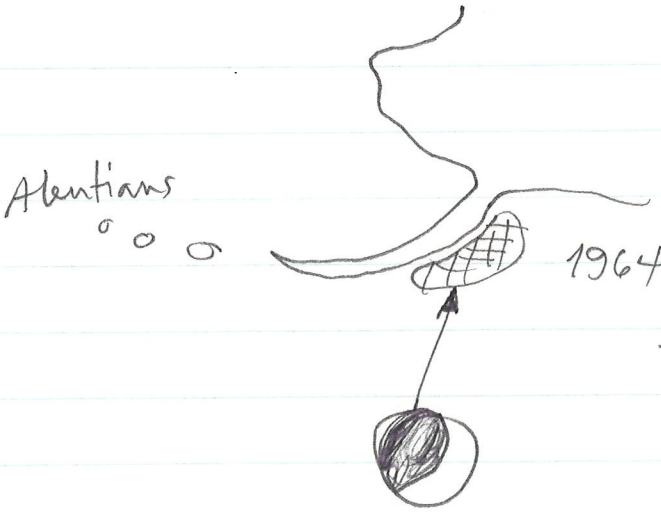

Two possibilities:

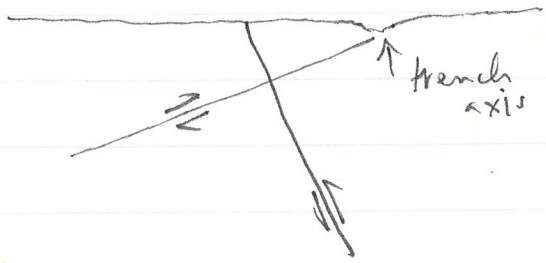

Clearly shallow angle thrusting rather than steeply dipping is preferred

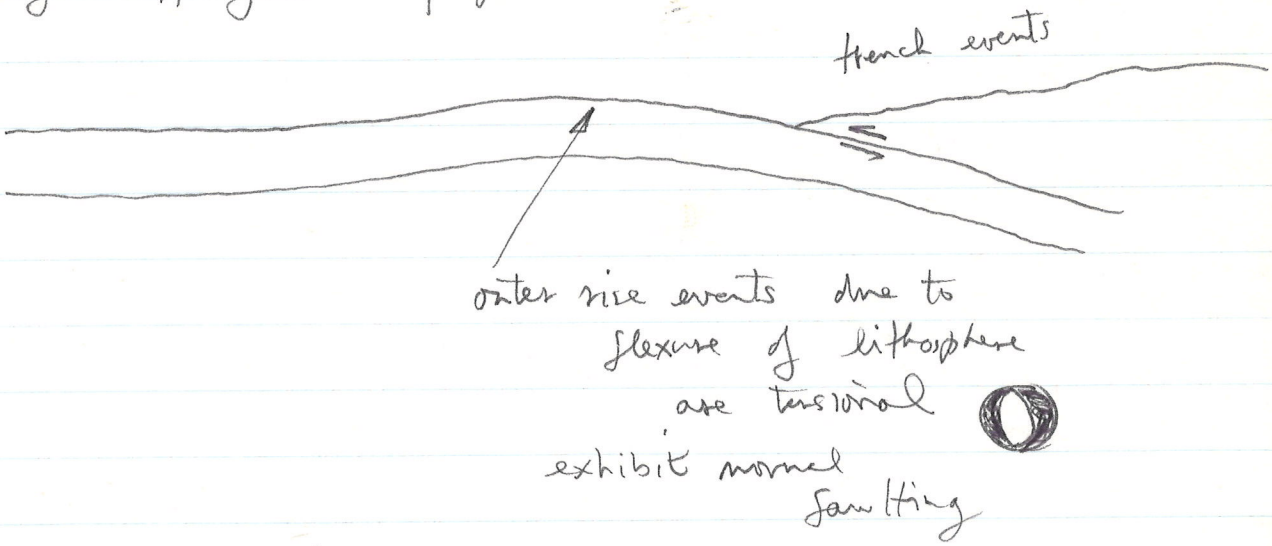

The amplitudes of P waves on the focal sphere: it can be shown that they are (for a pt. source quake) the same as those generated by a hypothetical so-called double couple

acting in the absence of any faulting

equivalent to

the two sets of forces exert no net torque

The double couple radiation pattern on the focal sphere is $\propto$ to

$$\boxed{\mathcal{R} \propto (\hat{r}\cdot\hat{n})(\hat{r}\cdot\hat{e})}$$

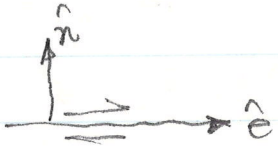

$\hat{e}$ = slip direction
$\hat{n}$ = fault normal
$\hat{r}$ = unit vector to pt. on focal sphere

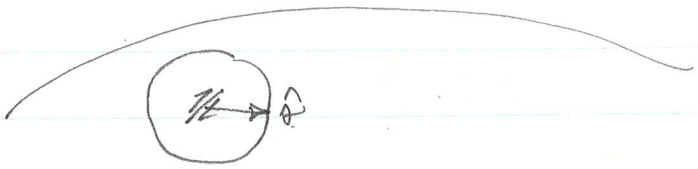

Note $\mathcal{R} = 0$ on fault plane and on auxiliary plane; these the two nodal planes of the focal mechanism solution

It is also customary to define 3 axes P, T, B

B: the int. axis is along the fault – auxiliary plane intersection

P: the comp. axis is in the 2 dilatational quadrants where R is the greatest

T: the tensional axis is in the 2 compressional quadrants where R is the least (or the greatest negative)

Deep focus quakes in slabs: no tendency for alignment of planes but P axes tend to point downdip: interpreted as due to the resistance of the slab to subduction.

Shudofsky used modern approach in E. Africa: surface waves (bigger ⇒ smaller events) + body wave modelling

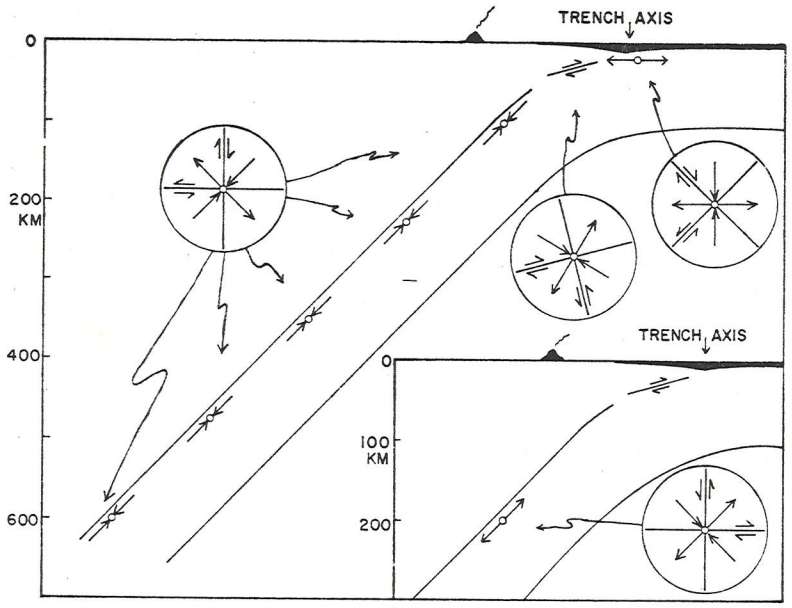

Fig. 11. Vertical sections perpendicular to the strike of an island arc showing schematically typical orientations of double-couple focal mechanisms. The horizontal scale is the same as the vertical scale. The axis of compression is represented by a converging pair of arrows; the axis of tension is represented by a diverging pair; the null axis is perpendicular to the section. In the circular blowups, the sense of motion is shown for both of the two possible slip planes. The features shown in the main part of the figure are based on results from the Tonga arc and the arcs of the North Pacific. The insert shows the orientation of a focal mechanism that could indicate extension instead of compression parallel to the dip of the zone.

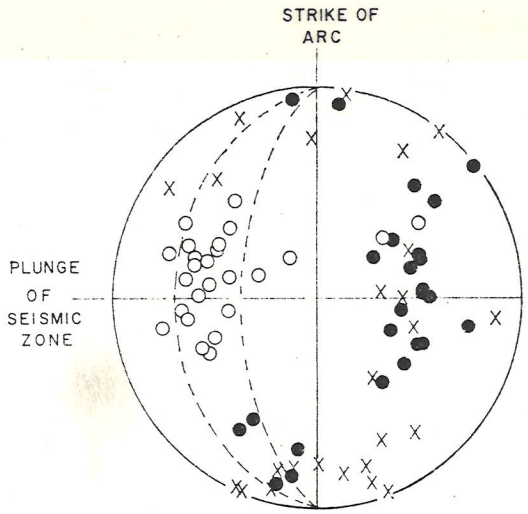

Fig. 10. Orientations of the axes of stress as given by the double-couple focal mechanism solutions of deep and intermediate earthquakes in the Tonga arc, the Izu-Bonin arc, and the North Honshu arc. Open circles are axes of compression, P; solid circles are axes of tension, T; and crosses are null axes, B, all plotted on the lower hemisphere of an equal-area projection. The data, selected from available literature as the most reliable solutions, are taken from *Isacks and Sykes* [1968], *Honda et al.* [1956], *Ritsema* [1965], and *Hirasawa* [1966]. The data for each of the three arcs are plotted relative to the strike of the arc (Tonga arc, N 20°E; Izu-Bonin, N 15°W; North Honshu arc, N 20°E). The dips of the zones vary between about 30° and 60°, as indicated by the dashed lines in the figure. Note the tendency of the P axes to parallel the dip of the seismic zone and the weaker tendency for the T axes to be perpendicular to the zone.

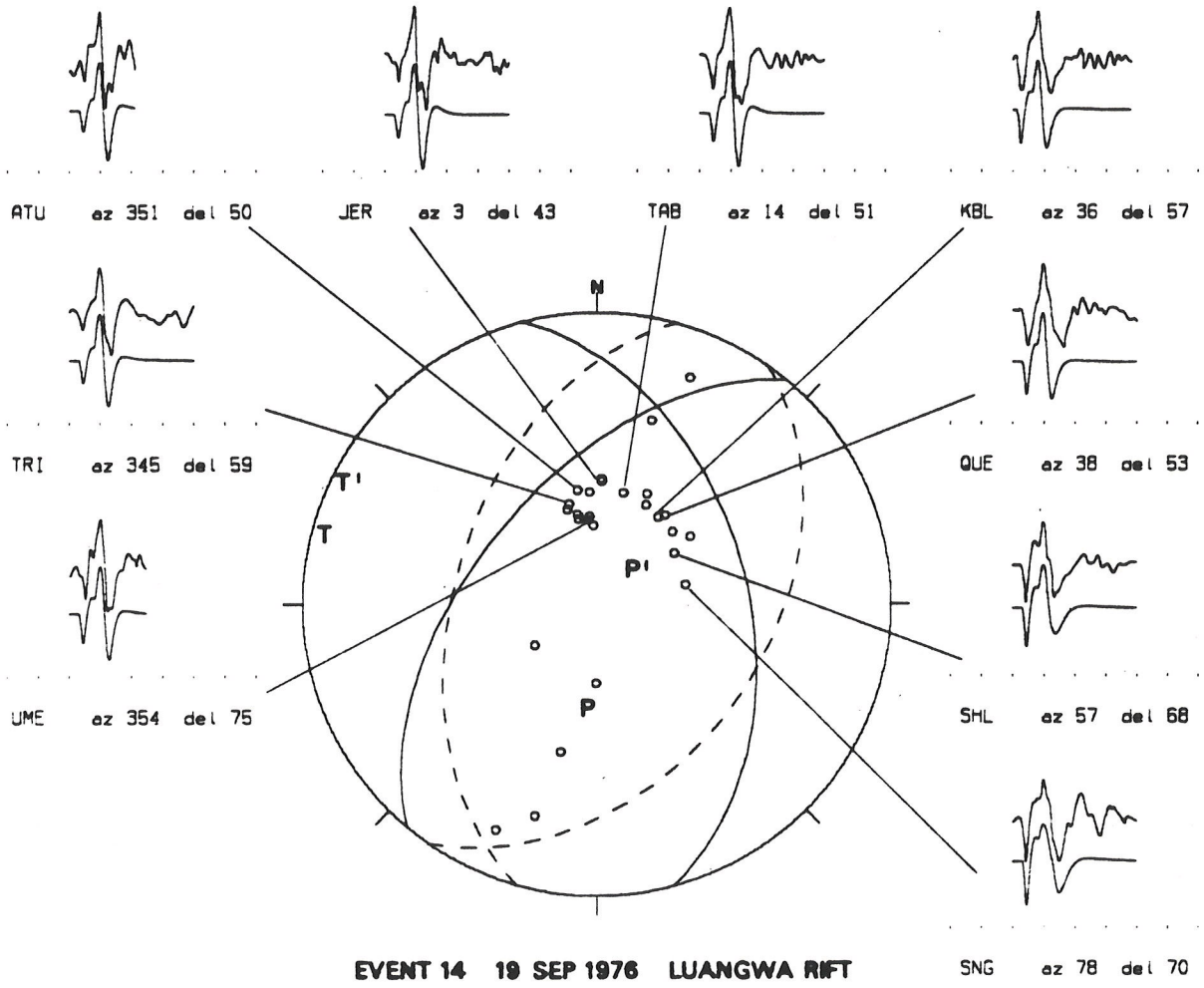

Fig. 18. Comparison of observed and synthetic long-period P waves for Event 14. See Figure 7 for explanation of symbols. The focal depth from body wave modelling is 25 km.

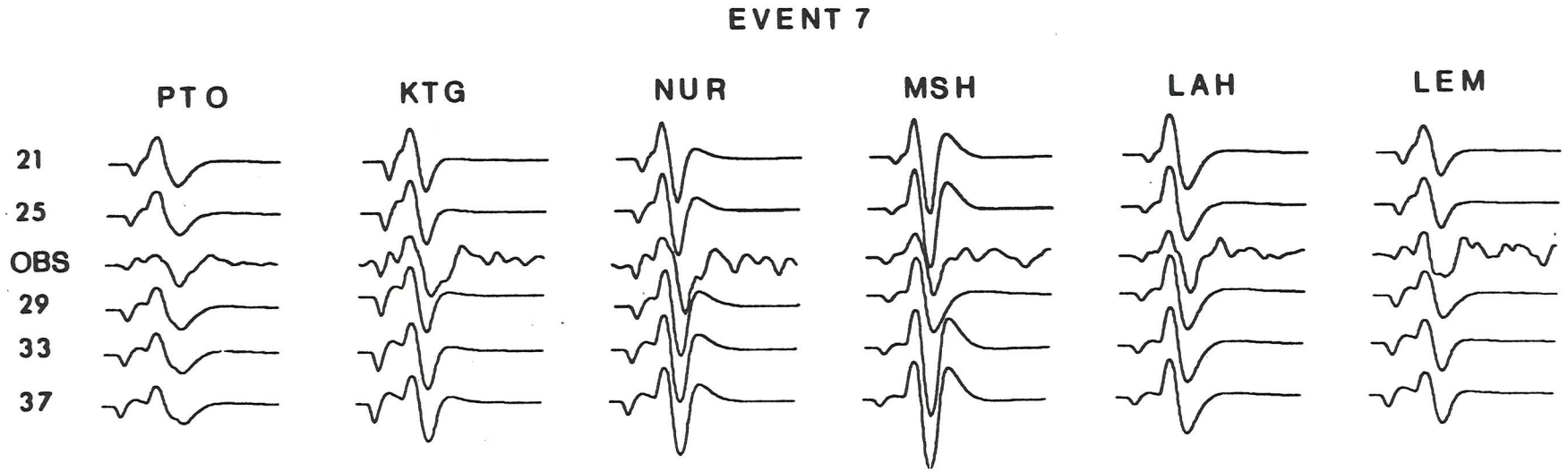

Fig. 13. Variation of the synthetic waveforms with focal depth for Event 7 and comparison with observed signals.

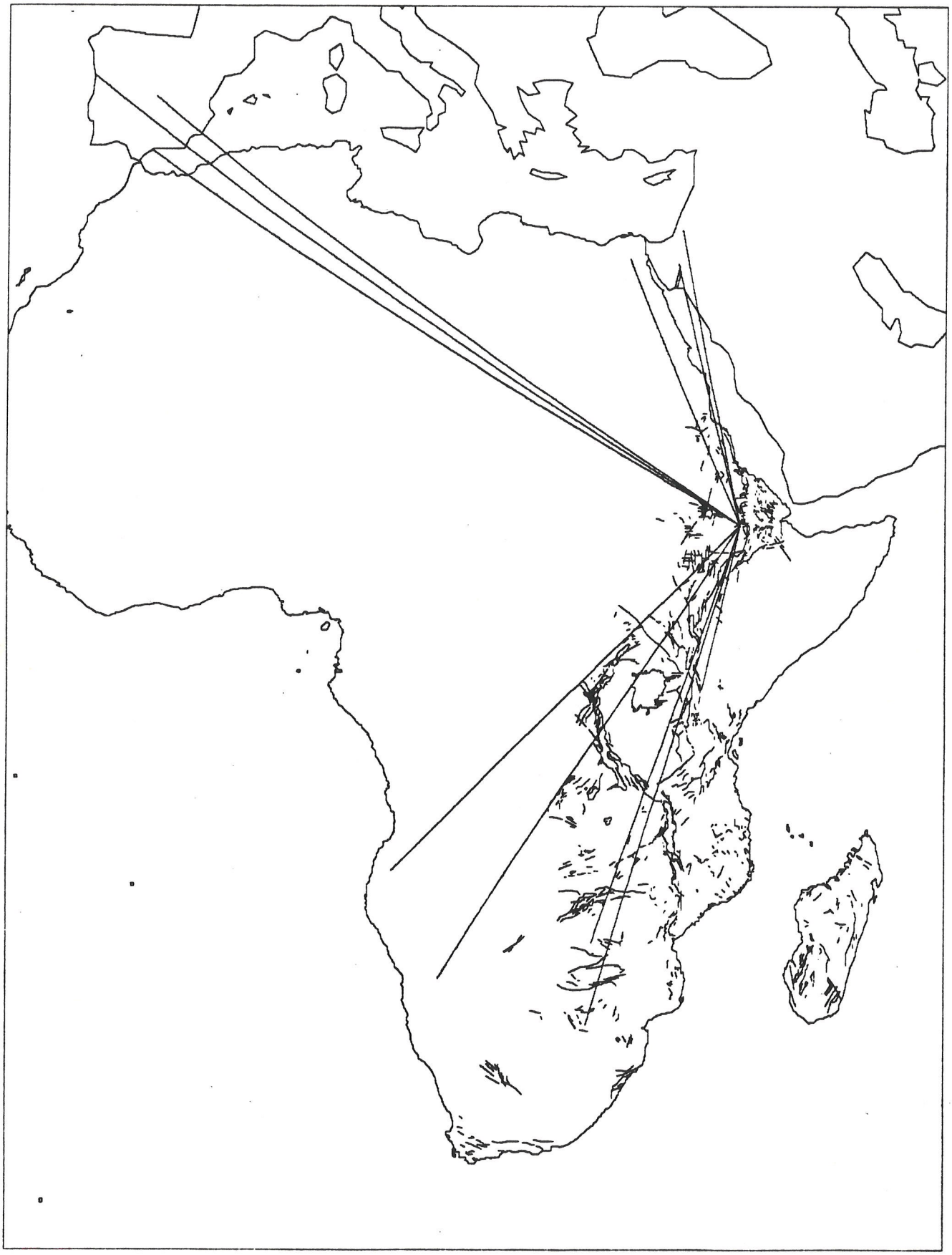

Fig. 3a. Rayleigh wave travel paths from Ethiopian reference point.

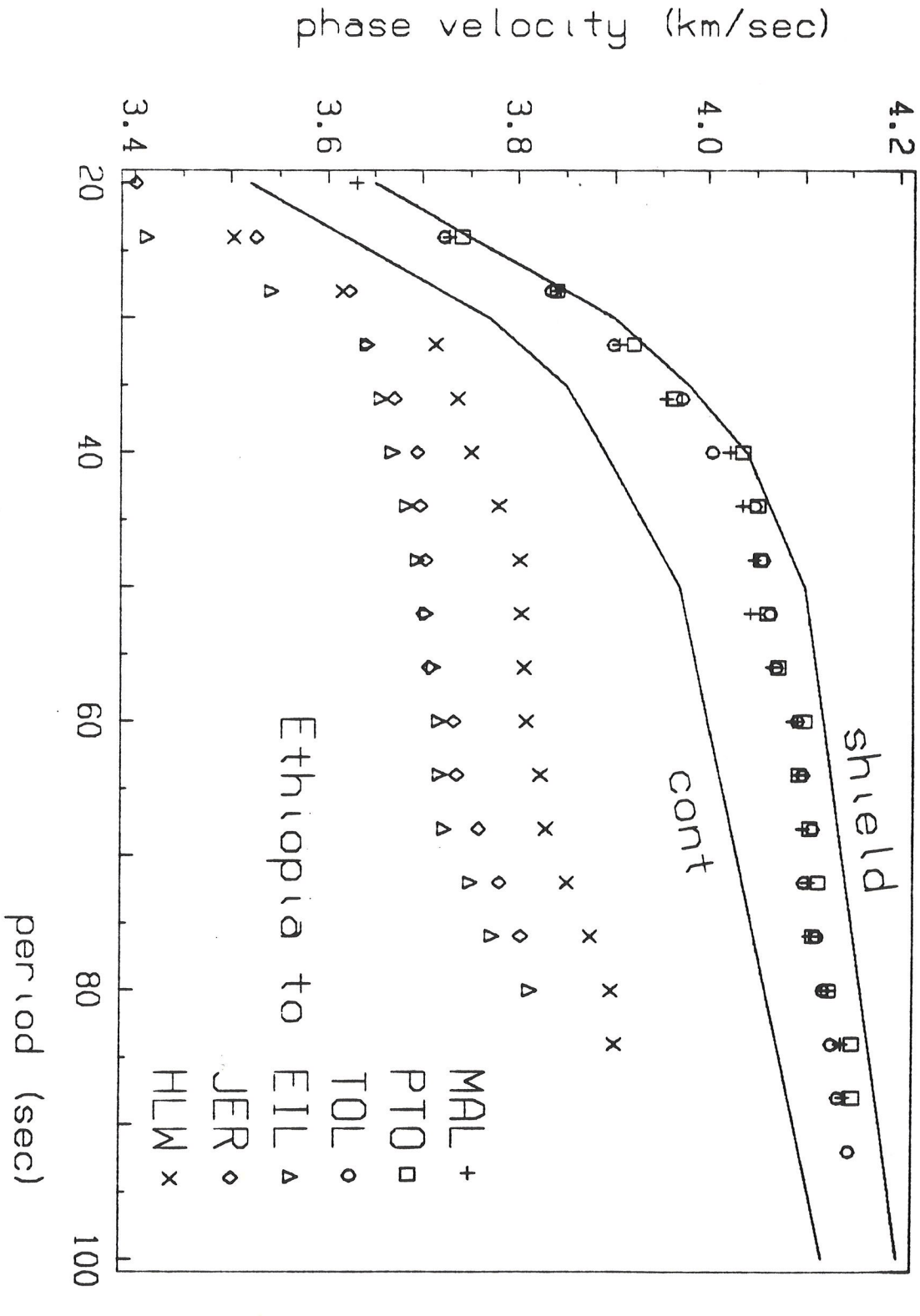

Fig. 3b. Phase velocities from Ethiopian reference point

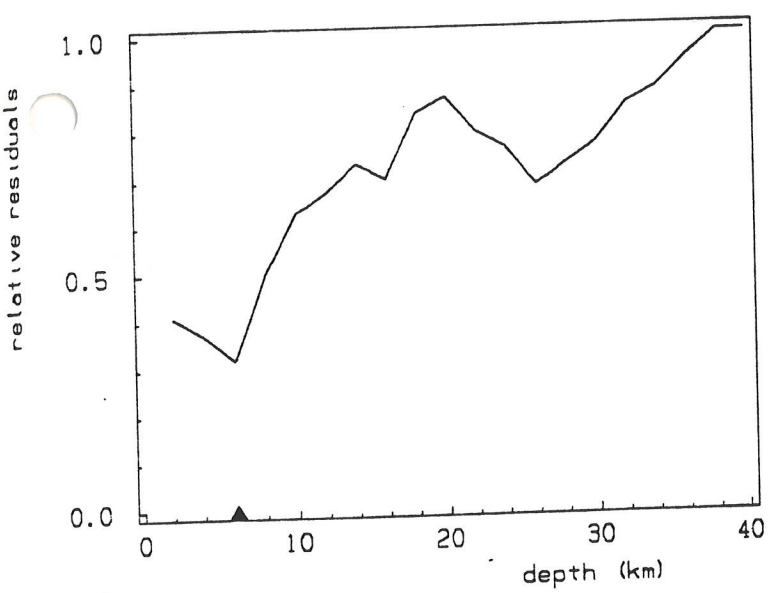

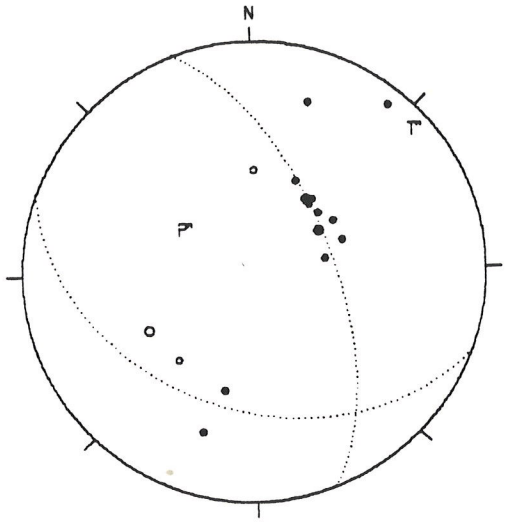

Fig. 4e EVENT 5 13 FEB 1972 TANZANIA

EVENT 5
13 FEB 1972
TANZANIA
STRIKE = 160
DIP = 62
SLIP = 241
DEPTH = 6
LOG MOMENT = 24.06

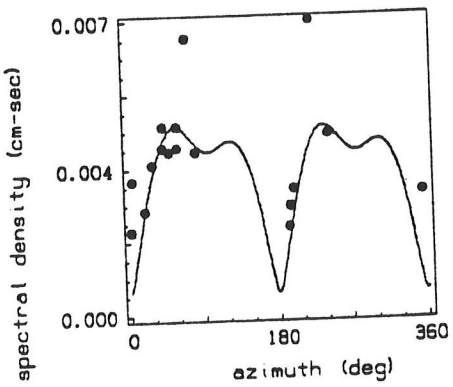

65 sec

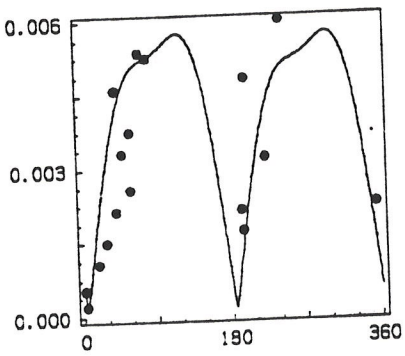

55 sec

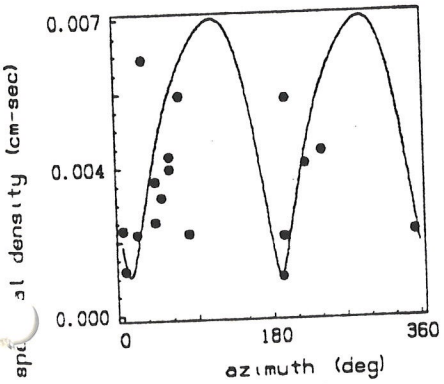

45 sec

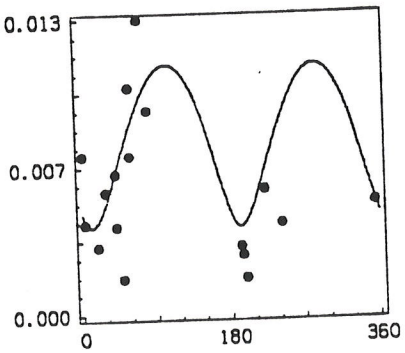

35 sec

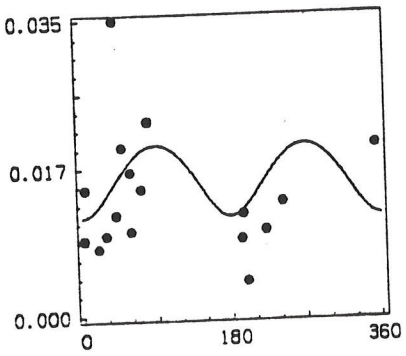

25 sec

Fig. 5e

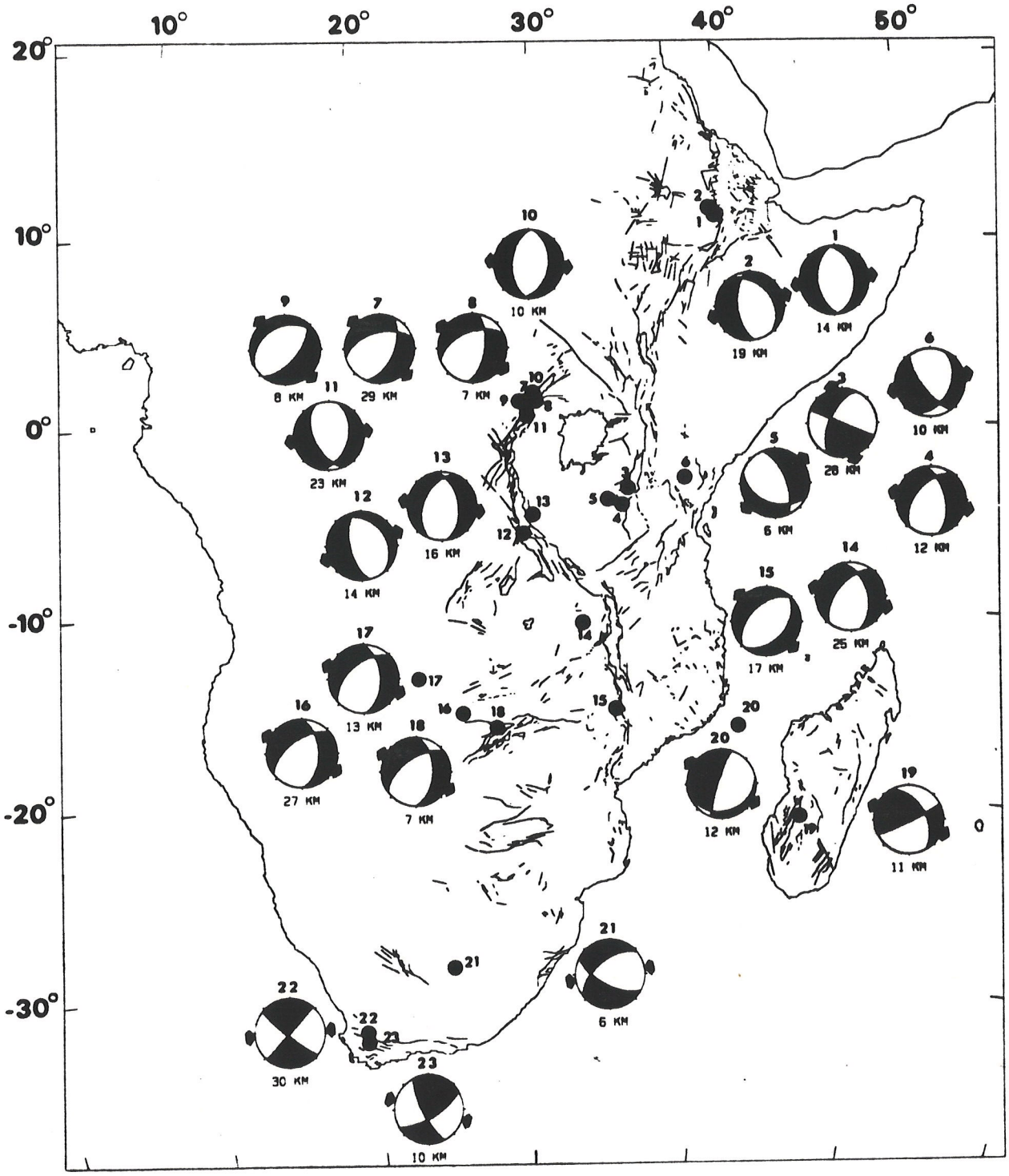

Fig. 28. Epicentral locations, source mechanisms, and focal depths of the 23 events studied in this paper. Outward-facing arrows indicate the direction of the horizontal projection of least compressive stress axes. Inward-facing arrows for the three southernmost events indicate greatest compressive stress axis directions.

Lecture on earthquake mechanics

[redacted]

We now consider the finite nature of earthquake sources.

H. F. Reid 1911 formulated elastic rebound hypothesis. Surveying: triangulation nets resurveyed after 1906 San Francisco earthquake

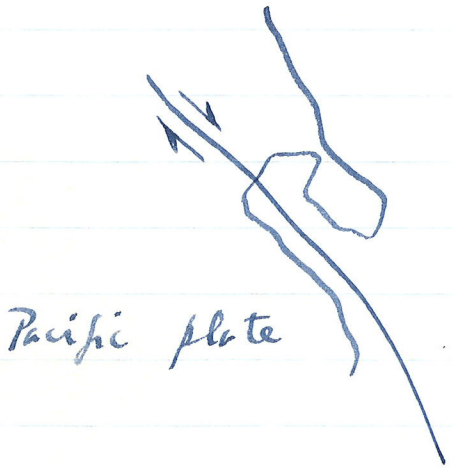

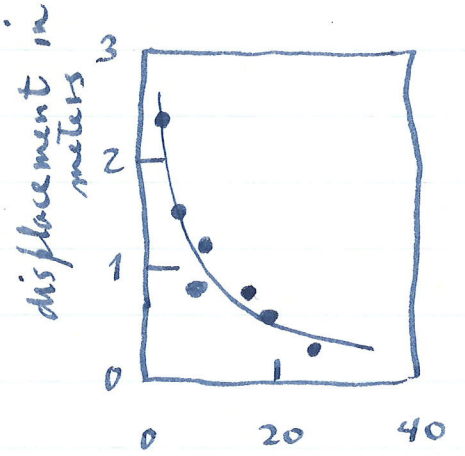

This is an inverse picture of the elastic strain released by the earthquake.

Consider an imaginary straight fence long before 'quake.

plates are moving; strain builds up

Then failure occurs when strength of fault zone is exceeded

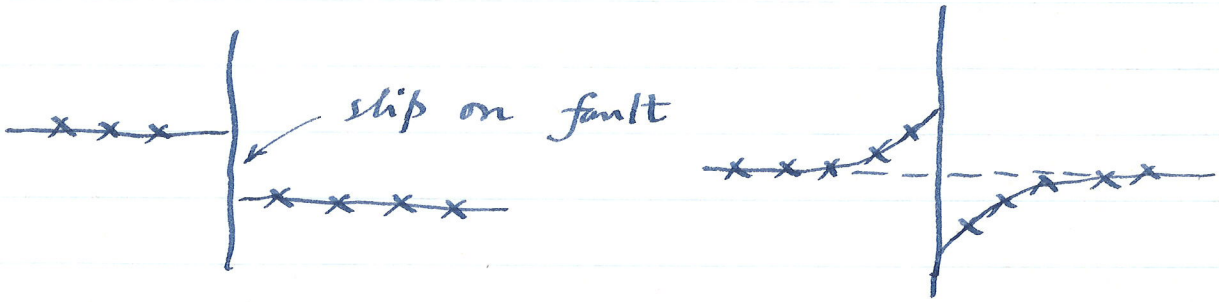

a <u>straight</u> fence at $t = 0-$ would get bent like this

The slippage relieves the shear stress on the fault.

Say the <u>stress level</u> <u>drops</u> <u>uniformly</u> on the rupture surface from σ_1 to σ_2 dyne/cm^2.

<u>Stress drop</u> $\Delta\sigma = \sigma_1 - \sigma_2$: a fundamental seismological variable.

Mathematical problem: half-space initially has shear stress σ_1 everywhere (at all depths)

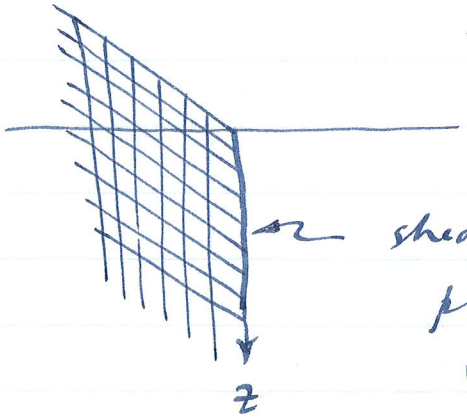

shear stress on fault plane σ_1: rock on west pulling rock on east to the north.

Now suppose stress drops by $\Delta\sigma$ down to a depth h

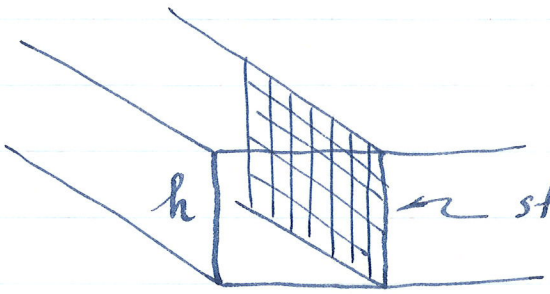

stress drop $\Delta\sigma = \sigma_1 - \sigma_2$

What is displacement everywhere. This an elastic mixed boundary value problem. First solved in seismological context by Kasahara 1957 and Knopoff 1958 GJRAS, 1, 44-52. Bull. E. R. Inst. Tokyo, 35, 473-532.

Answer: for displacement on fault surface

Each side slips by $(\Delta\sigma/\mu)(h^2-z^2)^{1/2}$
Total slip is twice this

$$\Delta s(z) = (2\Delta\sigma/\mu)(h^2-z^2)^{1/2}$$

μ = rigidity

On surface of ⊕:

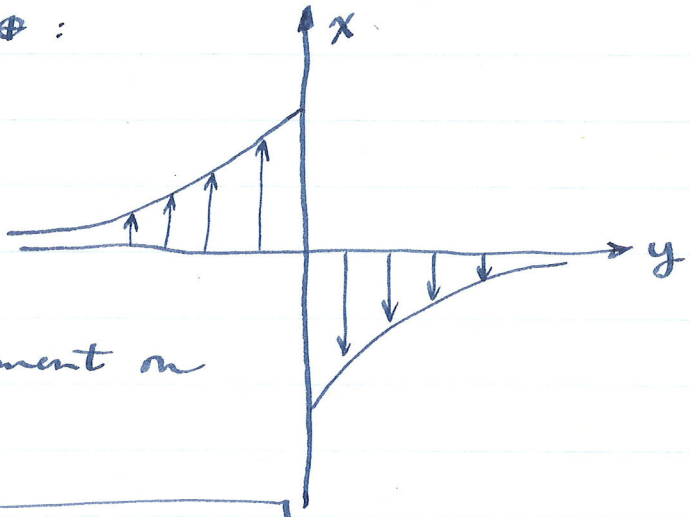

form of displacement on each side is

$$(\Delta\sigma/\mu)\left[(h^2+y^2)^{1/2} - y\right] \quad *$$

Note: for $y=0$, this is $(\Delta\sigma/\mu)h$
and for $y \to \infty$ this $\to 0$

The total offset at the surface is, from either formula, $\Delta s_0 = 2(\Delta\sigma/\mu)h$

Can fit a function of form * to survey data.

The slip $\underline{\Delta s_0 \sim 5 \text{ meters}}$. One gets the result $\underline{h \sim 6 \text{ km}}$. The length of faulting was $\sim$ 500 km.

The very shallow depth dictated by the falloff of the geodetic displacement at distances a few 10's of km from the fault trace. Consistent with seismicity (of microearthquakes) in California — all very shallow 5–10 km.

What is stress drop $\Delta\sigma = \Delta s_0 \mu / 2h$

$= (500)(3 \cdot 10^{11}) / 2(6 \cdot 10^5) =$

$1.2 \cdot 10^8$

(μ: typical crustal rigidity)

$$\boxed{\Delta\sigma \sim 120 \text{ bars}}$$

This a typical value found for crustal earthquakes $\Delta\sigma \sim 100$ bars.

Note: an important fact: only $\Delta\sigma$ is experimentally accessible by seismological or geodetic measurements. The absolute level of stress σ_1 cannot be inferred.

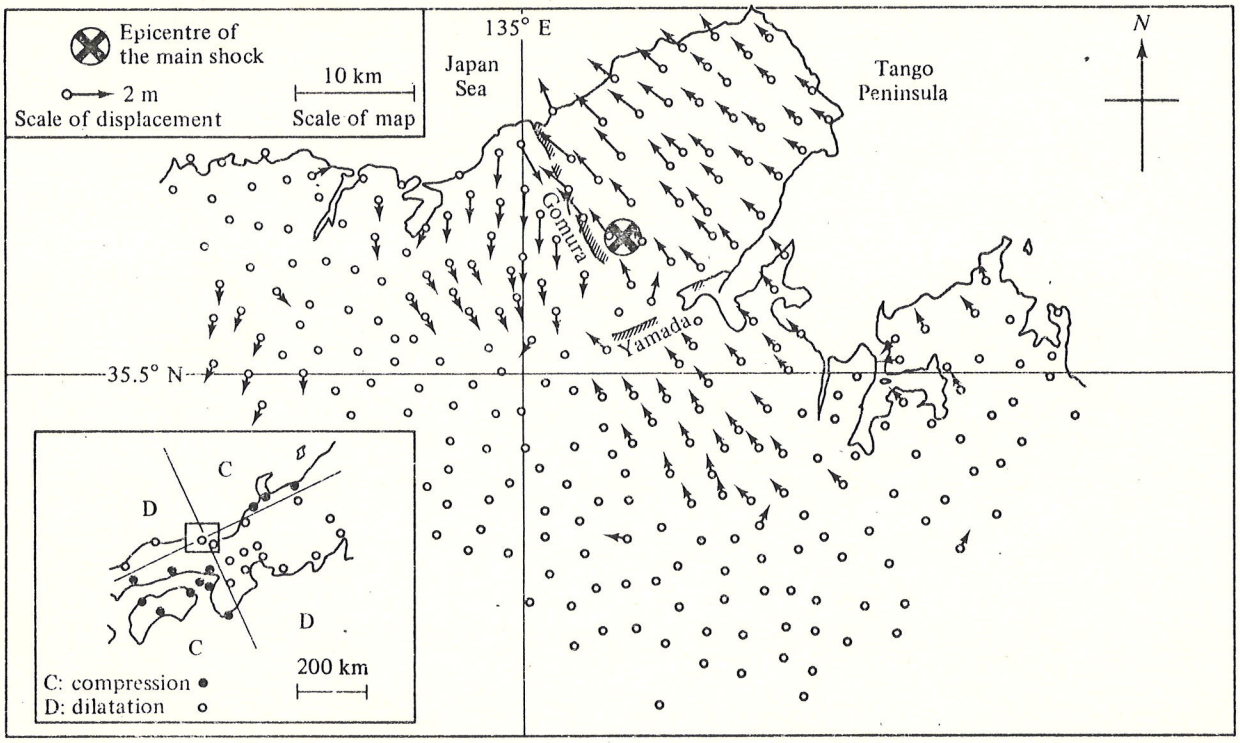

Fig. 4.5. Displacement of triangulation points (Land Survey Department, 1930) in the Tango earthquake of 1927. The distribution of P-wave first motions (Honda, 1932) in the inset shows the radiation pattern. (From Kanamori, 1973. Reproduced, with permission, from the *Annual Review of Earth & Planetary Sciences*, Volume 1. © 1973 by Annual Reviews Inc.)

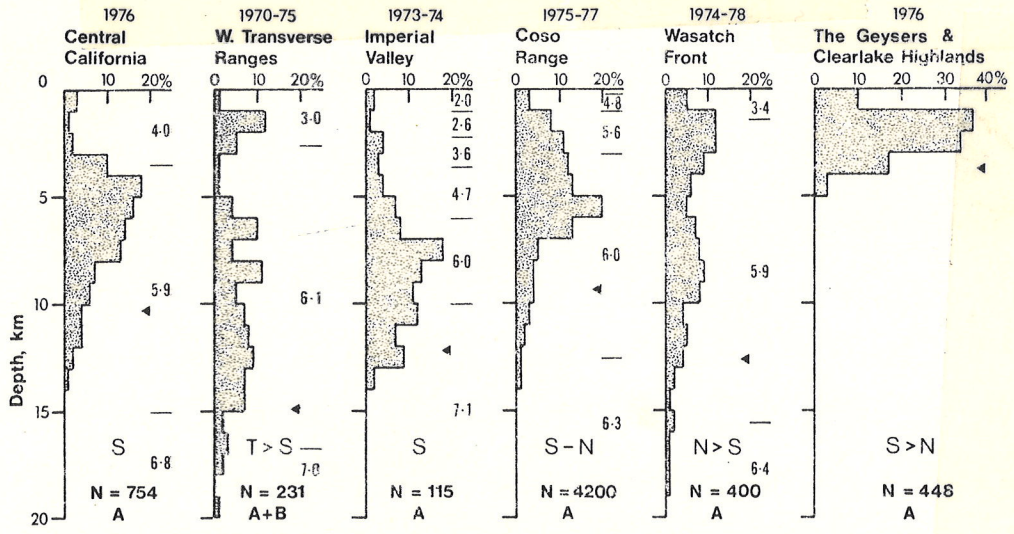

FIG. 2. Depth distribution of microearthquakes in the sampling areas. *P*-wave velocities (km/sec) for the crustal models used in location are given on the *right* of the histograms and the depth above which 90 per cent of the activity occurs is indicated by the solid triangles; the dominant faulting mode (T = thrust, S = strike-slip, N = normal), the number of microearthquakes in the sample, and the quality of the data are listed at the base.

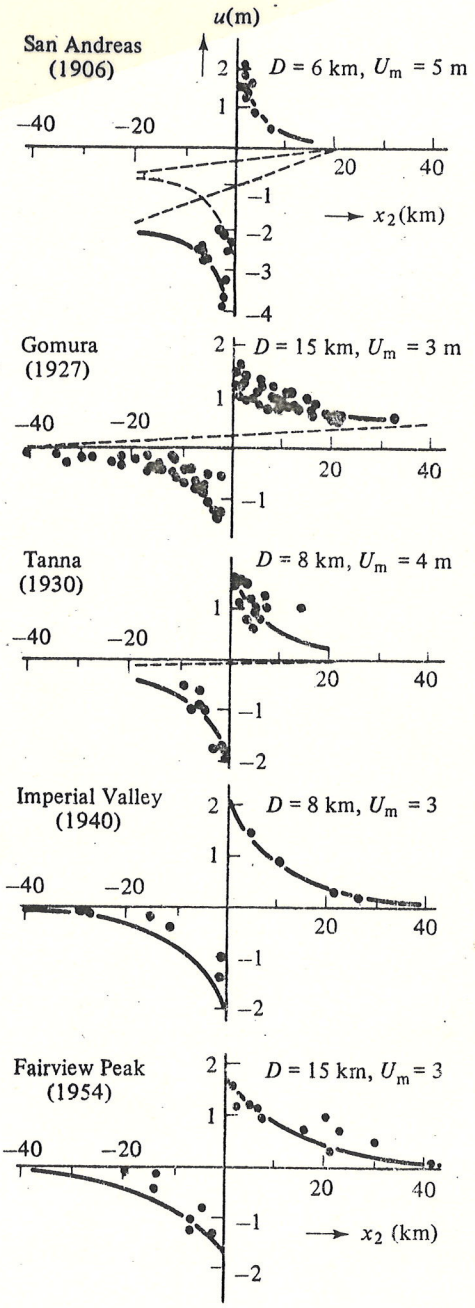

Fig. 4.9. Surface displacements (parallel to the fault strike) associated with several representative strike-slip faults for comparison with the predictions of the vertical strike-slip model (fig. 4.7). Broken lines show corrections for the hypothetical strain accumulation during the period between pre- and post-earthquake surveys. (After Kasahara, 1960.)

An important seismological parameter is the <u>seismic moment</u>, defined by

$$M_0 = \mu A \bar{\Delta s}, \quad A = \text{fault area}, \quad \bar{\Delta s} = \text{average slip}.$$

In this model $\bar{\Delta s} = \frac{\pi}{4} \Delta s_{max}$

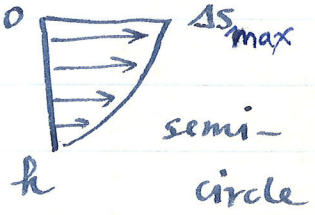

$$M_0 = 3 \cdot 10^{11} (6 \cdot 500) \cdot 10^{10} \cdot \frac{\pi}{4} \cdot 5 \cdot 10^2$$

$$\boxed{M_0 \cong 4 \cdot 10^{27} \text{ dyne-cm}}$$

A major strike-slip event, but thrust events can be 2 orders of magnitude larger. Seismic moment is a routinely measured parameter for large events — the best measure of the size of an earthquake.

The <u>energetics of earthquakes</u>: can ask the following question. Prior to an earthquake there is an amount of stored elastic energy given by

$$E_0 = \frac{1}{2} \int_V c_{ijke} \sigma^1_{ke} \sigma^1_{ij} \, dV$$

σ^1 initial strain

After the 'quake this has been released. The net elastic energy release is

$$\Delta E = \frac{1}{2} \int_V C_{ijke} \left(\sigma_{ij}^{1} \sigma_{ke}^{1} - \sigma_{ij}^{2} \sigma_{ke}^{2} \right) dV$$

Gauss' theorem enables one to write this as

$$\boxed{\Delta E = \frac{1}{2} (\sigma_1 + \sigma_2) \, \bar{\Delta s} \, A}$$

$\bar{\sigma} = \frac{1}{2}(\sigma_1 + \sigma_2)$ is the <u>average shear stress</u>.

Note: the energy release does <u>not</u> depend only on the stress drop but on the initial stress σ_1. It is, however, experimentally inaccessible by purely seismological methods.

The energy balance equation can be written as

$$\boxed{\Delta E = E_s + E_{ft} + E_{\text{crack tip}}}$$

E_s: radiated away as elastic waves to be ultimately dissipated elsewhere in ⊕.

E_{fr} : work done by friction on walls of fault during faulting — this heats up the walls of the fault

$E_{fr} \sim \sigma_{fr} \bar{\Delta s} A$, where σ_{fr} is the frictional stress acting during slip

$E_{crack\ tip}$: work done at crack tip in creating fresh fault area

$E_{crack\ tip} \sim G A$, where G is the effective shear fracture energy

Wong, JGR, 87, 990–1000 (1982) : G for Westerly granite $\sim 10^4$ J/m^2 or 10^7 erg/cm^2
Thus $E_{crack\ tip}$ for the San Francisco event can be estimated as

$$E_{crack\ tip} \sim 6 \cdot 500 \cdot 10^{10} \cdot 10^7 \sim 3 \cdot 10^{23} \text{ ergs}$$

, if it was really fracturing fresh Westerly granite. If this calculation is indicative, $E_{crack\ tip}$ could be important in faulting. It has been customary, however, to

ignore it in the past. In that case one can write for the radiated seismic energy

$$E_s = \Delta E - E_p$$
$$= \bar{\Delta s}\, A \left[\tfrac{1}{2}(\sigma_1 + \sigma_2) - \sigma_f \right]$$
$$= \bar{\Delta s}\, A \left[\tfrac{1}{2}(\sigma_1 - \sigma_2) + (\sigma_2 - \sigma_f) \right]$$

$$E_s = \tfrac{1}{2} \Delta\sigma\, A\, \bar{\Delta s} + (\sigma_2 - \sigma_f)\, \bar{\Delta s}\, A$$

It is also commonly assumed that faulting stops when the stress drops to the frictional value, in which case

$$\boxed{E_s = \tfrac{1}{2} \Delta\sigma\, A\, \bar{\Delta s}}$$

For the SF 1906 event:

$$E_s = \tfrac{1}{2} \cdot 120 \cdot 3 \cdot 10^{13} \cdot \tfrac{\pi}{4} \cdot 500 \cdot 10^{6}$$

$$\boxed{E_s = 7 \cdot 10^{23} \text{ ergs}}$$

Note that, in general, $\boxed{E_s = \tfrac{1}{2} \dfrac{\Delta\sigma}{\mu} M_0}$

TABLE I. – *Ten greatest earthquakes during 1904-1976.*

Earthquake	Year	M_s	M_0 (dyn·cm)	M_w [a]	E (erg)
Chile	1960	8.3	$2.0 \cdot 10^{30}$	9.5	$1.1 \cdot 10^{26}$
Alaska	1964	8.4	$8.2 \cdot 10^{29}$	9.2	$4.0 \cdot 10^{25}$
Aleutian Islands	1957	8.25	$5.9 \cdot 10^{29}$	9.1	$2.8 \cdot 10^{25}$
Kamchatka	1952	8.25	$3.5 \cdot 10^{29}$	9.0	$2.0 \cdot 10^{25}$
Ecuador	1906	8.6	$2.0 \cdot 10^{29}$	8.8	$1.0 \cdot 10^{25}$
Aleutian Islands	1965	7.75	$1.3 \cdot 10^{29}$	8.7	$7.1 \cdot 10^{24}$
Assam	1950	8.6	$1.0 \cdot 10^{29}$	8.6	$5.0 \cdot 10^{24}$
Kuril Islands	1963	8.1	$6.7 \cdot 10^{28}$	8.5	$3.5 \cdot 10^{24}$
Chile	1922	8.3	$6.9 \cdot 10^{28}$	8.5	$3.5 \cdot 10^{24}$
Banda Sea	1938	8.2	$7.0 \cdot 10^{28}$	8.5	$3.5 \cdot 10^{24}$

(*a*) M_w is the magnitude derived from M_0 and is more adequate than M_s (surface wave magnitude) to represent the size of great earthquakes.

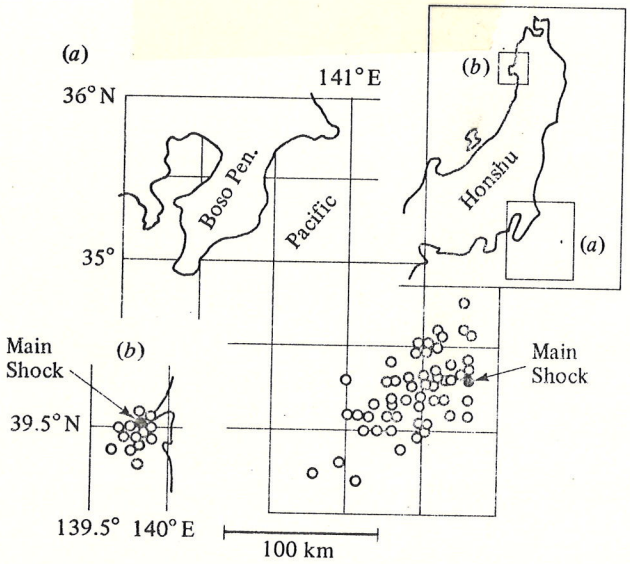

Fig. 2.3. Aftershock areas for earthquakes of different magnitudes: (*a*) off the Boso Peninsula, Honshu, Japan (1953, $M = 7.5$); and (*b*) on the Oga Peninsula, Honshu, Japan (1939, $M = 7.0$). (After Utsu & Seki, 1955.)

The so-called <u>seismic efficiency</u> is defined by

$$\eta = \frac{E_s}{\Delta E}$$

It gives the efficiency of the 'quake in radiating energy away. If $E_{crack\ tip}$ is indeed negligible, and if $E_2 = E_{fr}$, then

$$\eta = \frac{\Delta\sigma}{2\bar{\sigma}}$$

This also is not experimentally accessible inasmuch as $\bar{\sigma}$ can't be determined except by <u>in situ</u> means.

The largest quakes occur as thrust events in subduction zones. Kanamori gives a table of the 10 largest 'quakes 1904–76.
Example: 1964 Alaskan earthquake

$M_0 = 8 \cdot 10^{29}$ dyne-cm

$A \cong 200$ km $\times$ 1000 km

$\bar{\Delta s} \cong 10$ meters

For comparison, global heat flow is
$Q \sim 4 \cdot 10^{13}$ W $\sim 10^{28}$ ergs/yr.
Quakes $\sim$ 0.1–1% of Q (efficiency of $\oplus$ as heat engine)

For small to moderate events, a better model than that used for a long strike-slip event, as above, is:

Mathematical problem: Say slip $\Delta\sigma$ is released on a circular fault of radius a in an infinite homog. medium. What is resulting slip on fault? First determined, again in seismological context, by Keilis-Borok.

$$\Delta s(r) = \frac{2\Delta\sigma}{\mu C}\left(a^2 - r^2\right)^{1/2}$$

$$C = \frac{\pi}{4}\,\frac{2-\nu}{1-\nu}, \qquad \nu = \text{Poisson's ratio}$$

$\nu \sim \frac{1}{4}$ for typical crustal rocks, $C \sim \frac{7\pi}{12}$

$$\boxed{\Delta s(r) = \frac{24}{7\pi}\left(\frac{\Delta\sigma}{\mu}\right)\left(a^2 - r^2\right)^{1/2}}$$

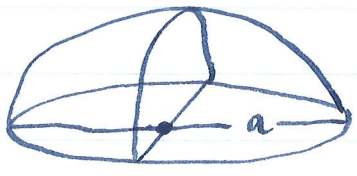

max at center; falls to zero slip at edges like a semicircle

The seismic moment is then

$$M_0 = \mu \int_0^a r\,\Delta s(r)\,dr \cdot 2\pi$$

r: Jacobian

2π from $\int_0^{2\pi} d\theta$

$$M_0 = \frac{16}{7} \Delta\sigma\, a^3$$

Or in terms of the fault area $A = \pi a^2$

$$M_0 = \frac{16}{7\pi^{3/2}} \Delta\sigma\, A^{3/2}$$

$$M_0 = 0.4\, \Delta\sigma\, A^{3/2}$$

or, in terms of logs

$$\log A = \frac{2}{3} \log M_0 - \frac{2}{3} \log (0.4\, \Delta\sigma)$$

If $\Delta\sigma$ is ~ constant, we'd expect $\log A \propto \frac{2}{3} \log M_0$.

How can these two quantities be measured?

M_0 is best measured using long-period surface waves or free oscillations. The amplitude of excitation of any wave whose wavelength $\lambda \gg$ source dimension a is directly $\propto M_0$. Thus, by measuring these amplitudes and taking attenuation and radiation patterns into account, one can measure M_0. Fault areas A can be

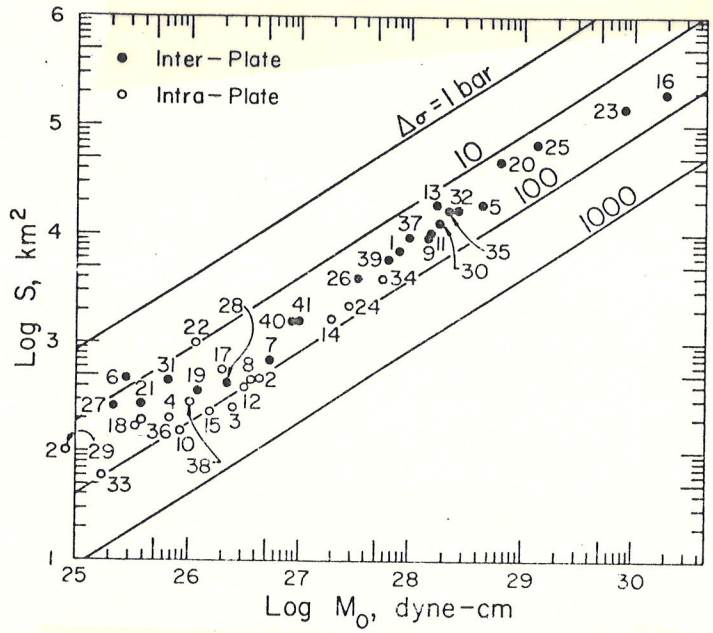

FIG. 2. Relation between S (fault surface area) and M_o (seismic moment). The straight lines give the relations for circular cracks with constant $\Delta\sigma$ (stress drop). The numbers attached to each event correspond to those in Table 1.

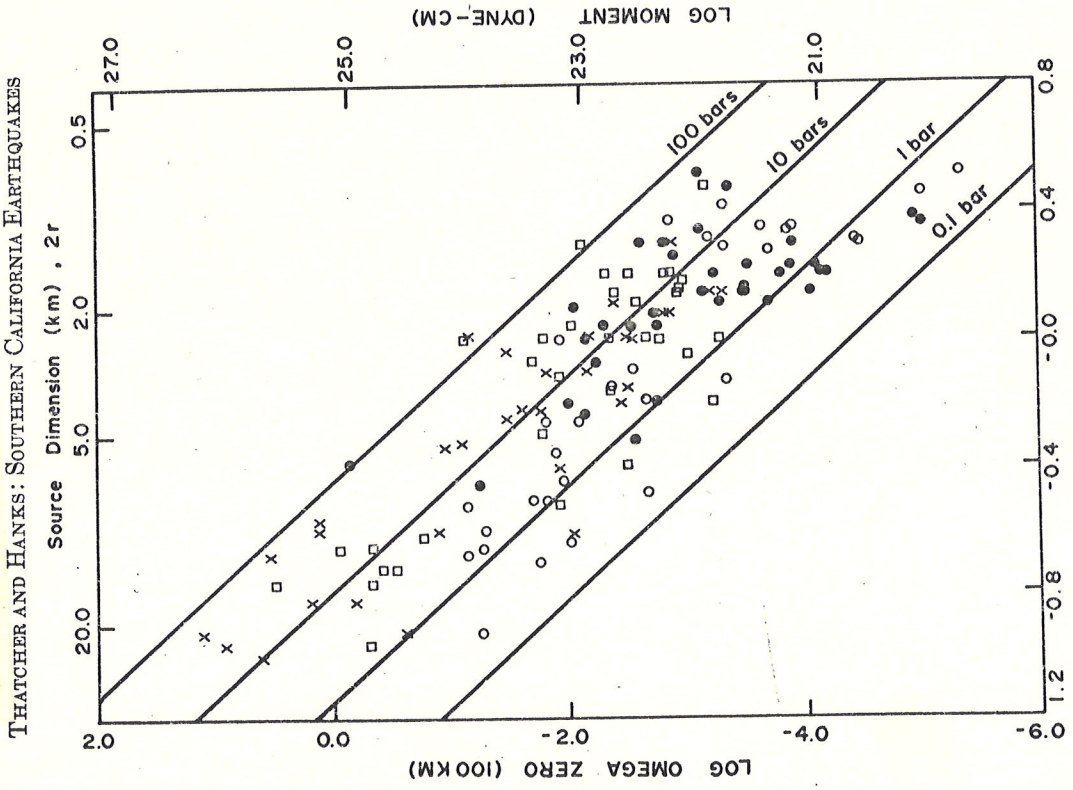

Fig. 6. Representation of Ω_o—f_o for all southern California earthquakes studied in this paper. The observed spectral quantities are shown scaled to source dimension $2r$ and seismic moment by using *Brune's* [1970] theory. Open circles represent earthquakes in offshore province and San Andreas fault; solid circles, in Transverse Ranges; squares, in Kern county; crosses, in other southern California locations.

estimated by finding the size of the aftershock region. This is believed to give a crude estimate. For small events another method is prevalent, which we'll discuss in a moment.

The agreement of the data from Kanamori + Anderson BSSA, 65, 1073–1095 is quite striking. Stress drops $\Delta\sigma$ in the range 10 – 100 bars seem to be indicated.

For smaller events a common way of measuring both M_0 and A (and thus $\Delta\sigma$) is to measure far-field P and S body wave spectra.

Theoretically, at frequencies low compared to the time it takes a seismic wave to traverse fault area

$$F(\omega) = [4\pi\rho c^3 r]^{-1} \mathcal{R}(\theta,\phi) M_0$$

α for P waves; β for S waves

double couple radiation pattern

At low freqs, the waves from all parts of the fault interfere constructively and the spectral amplitude is $\propto M_0$.

At higher frequencies, destructive interference sets in and one expects the spectrum to be smaller.

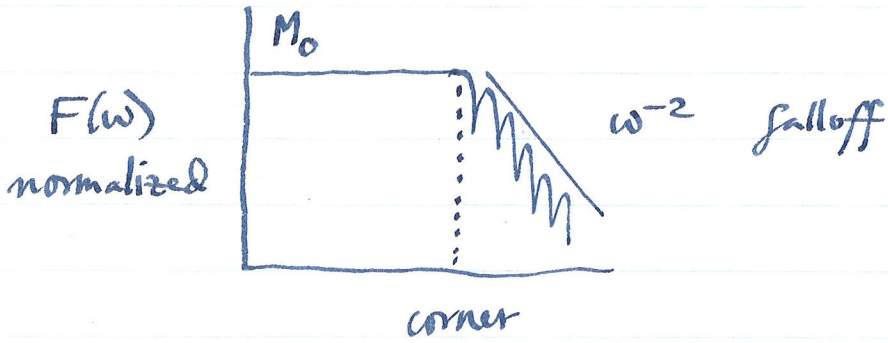

frequency: intersection of high and low-freq. trends.

The corner-frequency is inversely $\propto$ the fault dimensions. Smaller faults interfere constructively out to higher frequencies. An early theory for interpreting corner freqs. due to Brune, JGR, 75, 4997–5009 (1970). His a crude but essentially correct argument.

Madariaga (1976) solved BSSA, 65, 163–182 the problem of a

on expanding circular crack.

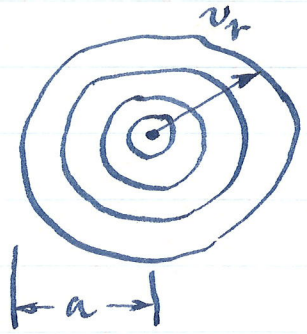

Nucleates at point, crack tip advances at rupture velocity $v_r < \beta$. Stress drop $\Delta\sigma$ is constant. Grows out to a radius a, stops suddenly.

He found the far-field high frequency radiation to be dominated by the stopping phases at times relative to the onset of rupture given by

$$\Delta t = a\left(\frac{1}{v_r} \pm \frac{\sin\theta}{c}\right)$$

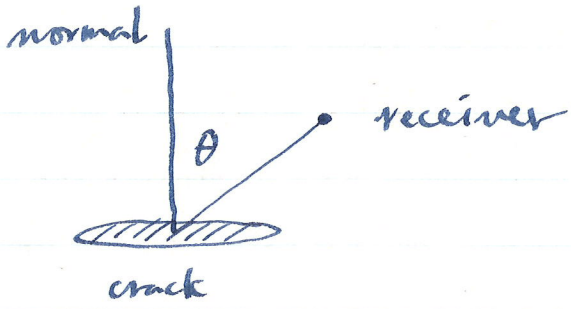

He finds that the corner frequencies, averaged for different rupture velocities and azimuths, are given by

$$f_0^P \approx 0.32\ \beta/a$$
$$f_0^S \approx 0.21\ \beta/a < f_0^P$$

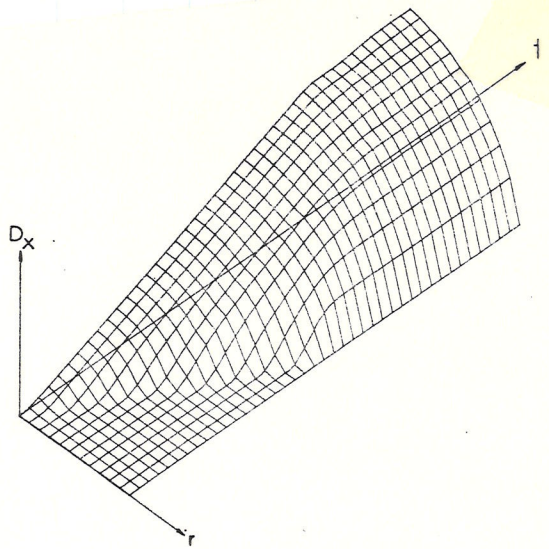

Figure 3
Source slip function for a circular fault with rupture velocity $v_R = 0.87\, v_s = 0.5\, v_p$. This plot shows the slip history as function of radius on the fault.

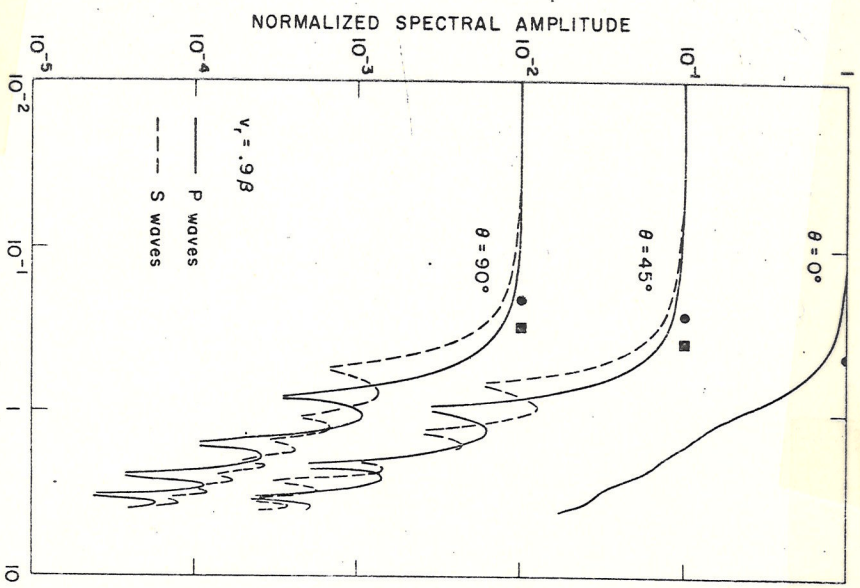

FIG. 8. Far-field spectrum of P and S waves radiated by a subsonic circular fault with $v_R = 0.9\beta$. The spectra for different θ are shifted by one decade in amplitude. The squares indicate the P corner frequencies while the circles indicate the S corner frequencies.

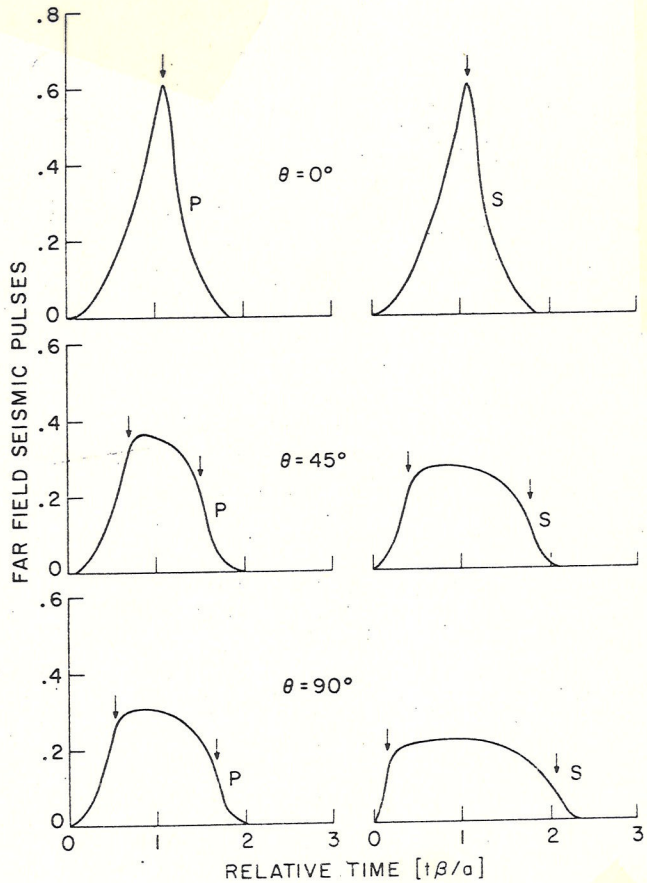

FIG. 9. Far-field displacement pulses radiated by a subsonic circular fault. Time is measured relative to the arrival from the nucleation point at the center of the fault. The arrows indicate the arrival time of stopping phases from the nearest and farthest points on the edge of the fault. The displacement pulses are scaled by a constant time integral (constant low-frequency level).

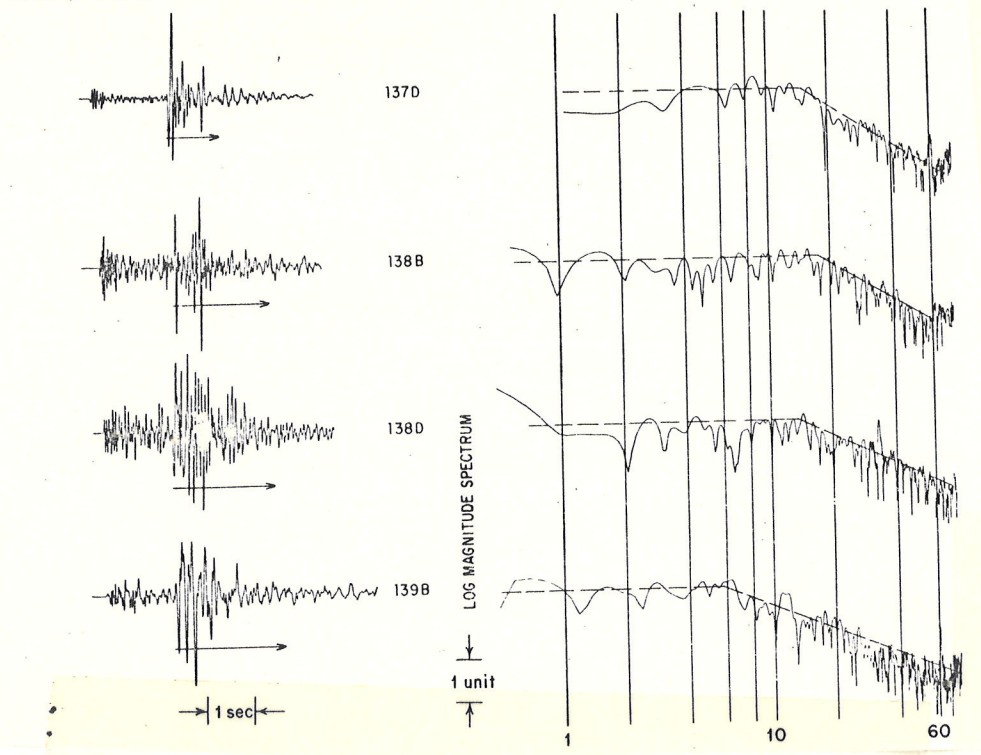

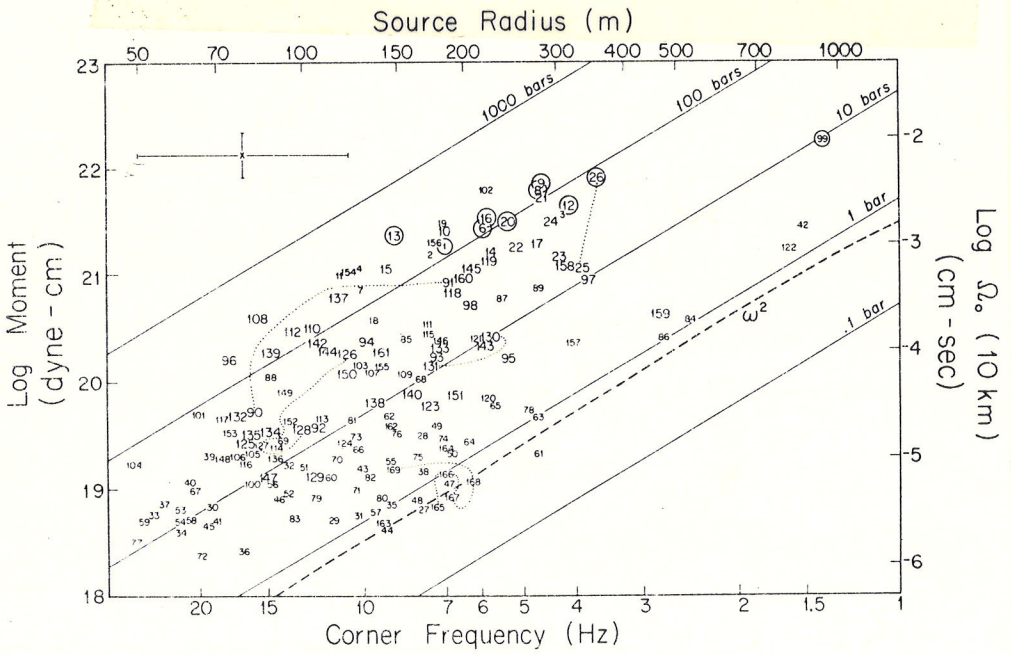

Figure 8. Log Ω_0 (10 km) is plotted against log f_c, where Ω_0 (10 km) = $\Omega_0 \cdot R/10$ and R is hypocentral distance in km. Also shown are axes for interpretations in terms of seismic moment, source radius and stress drop using the model of Brune – equations (3)–(5). Events are indicated by the ID numbers used in Table 1. Events which generated surface waves large enough to be observed at DUG or TUC have circled ID numbers. The moment–corner frequency relation for Aki's (1972) ω^2 model is indicated by the dashed line. Error bars refer to measurements of spectra of events which were recorded on only one instrument; these events have the smaller-sized ID numbers. Measurements of spectra of events which were recorded on two or more instruments (these events have the larger-sized ID numbers) were averaged and are thought to be more accurate. Some groups of events with extremely similar seismograms and spectra (ID numbers 25, 26; 90, 91; 130, 131; 126, 127, 128 and 165, 166, 167, 168, 169) are indicated by dotted lines which connect the members of each group. Because effects of radiation pattern, path attenuation and scattering must be similar for members of each such group, differences in f_c and Ω_0 for members of such a group are probably due to differences in source mechanism.

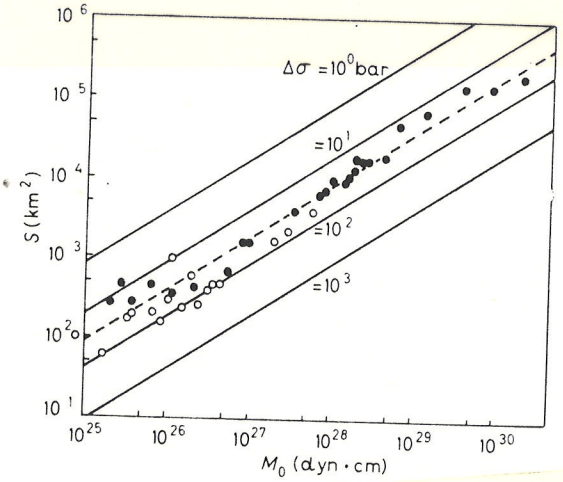

Fig. 5. – The relation between the fault area and the seismic moment. The solid lines are for constant stress drops, dashed line $M_0 = 1.23 \cdot 10^{22} S^{\frac{3}{2}}$ dyn·cm (S in km²); • interplate, ○ intraplate.

These formulae, or ones like them but with constants different than 0.32 and 0.21 have been used by Thatcher and Hanks for S. Calif. events and by Tucker and Brune for S. Fernando aftershocks as well as by many other workers.

The fundamental result from all these studies is that stress drops so inferred by seismologists in this way are in the range 10–100 bars over a very wide range of fault sizes from 50 meters to more than 1000 km, more than 5 orders of magnitude; 12 orders of magnitude in M_0.

These low stress drops seem to be in conflict with the measured laboratory properties of rocks. Can be illustrated by returning to strike-slip events on the San Andreas fault.

The frictional strength holding the faces together is, according to Byerlee's "law", for stresses < 2 kbar

$$S_{ft} = 0.85\ (1-\lambda)\ \rho g z$$

$$\lambda = \rho_{fluid} / \rho_{rock}$$

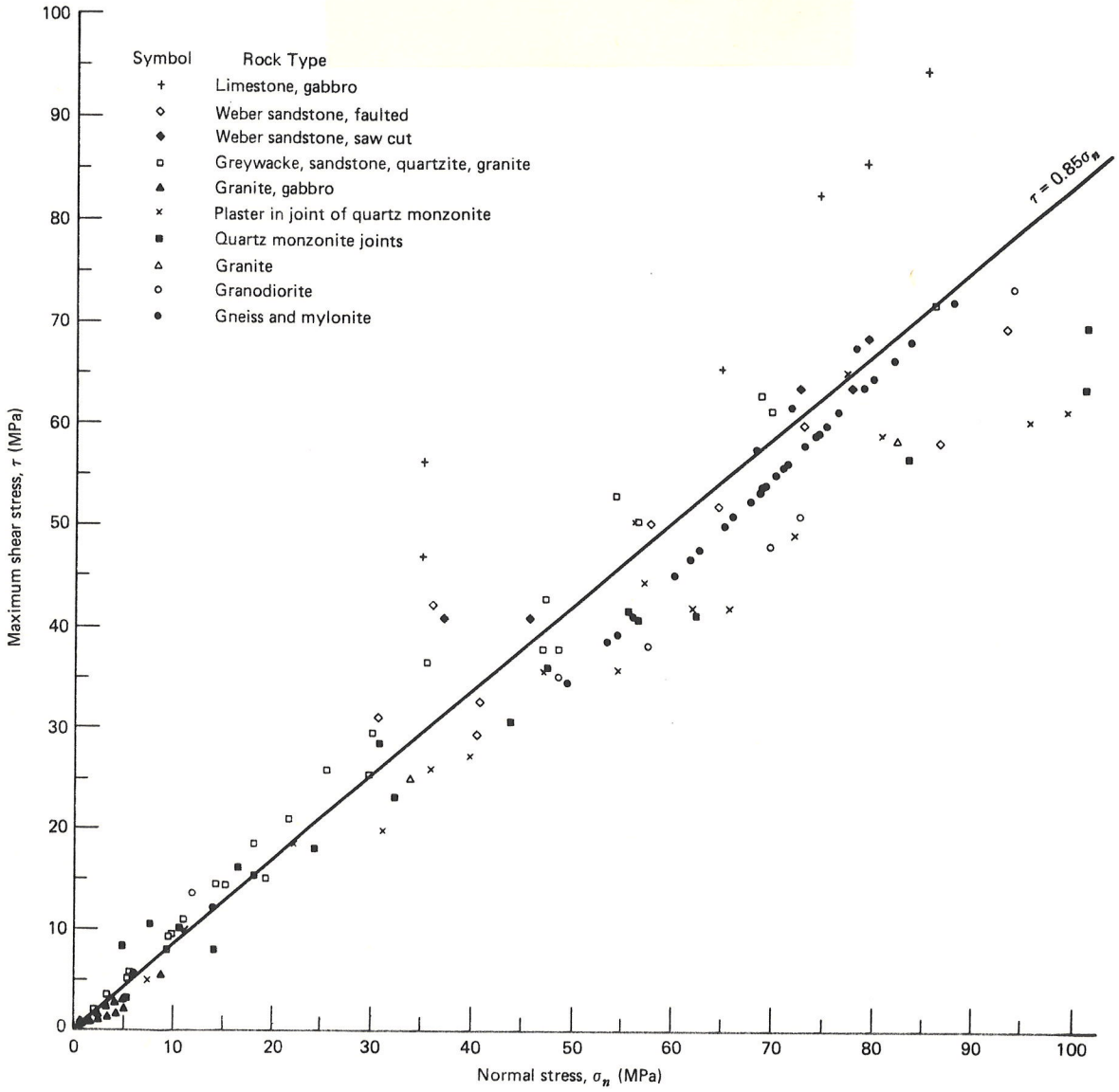

Figure 8-6 Maximum shear stress to initiate sliding as a function of normal stress for a variety of rock types. The linear fit defines a maximum coefficient of static friction max f_s equal to 0.85. Data from J. D. Byerlee, Friction of rocks, in *Experimental Studies of Rock Friction with Application to Earthquake Prediction*, ed. J. F. Evernden, pp. 55–77, U.S. Geological Survey, Menlo Park, Calif., 1977.

5. – Friction experiments on rocks.

BYERLEE [42] summarized the results of friction experiments on rocks, and showed that, at high normal stress, the friction is nearly independent of

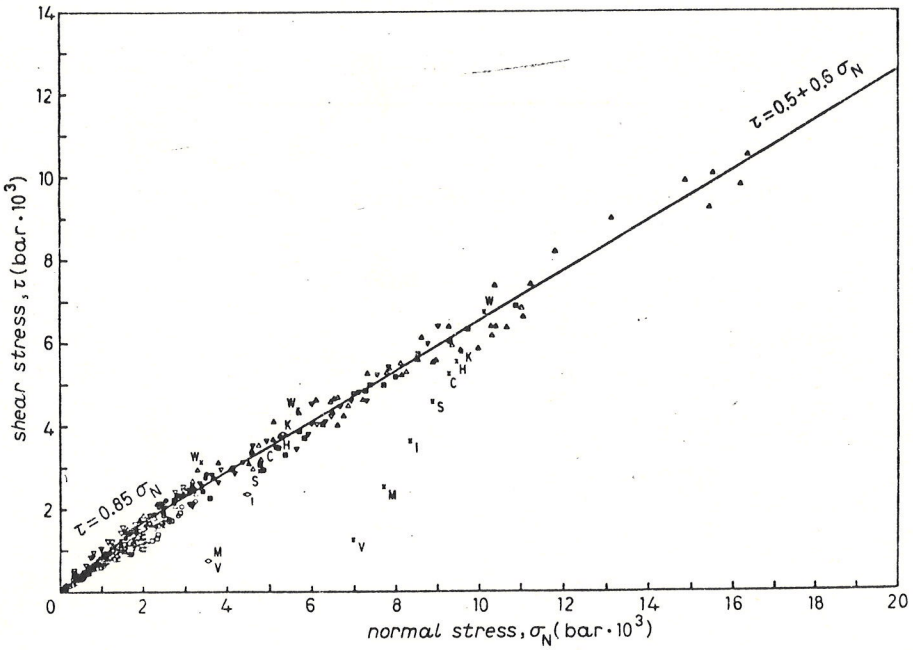

Fig. 8. – Shear stress plotted as a function of normal stress for a variety of rock types (after [42]): ▲ granite, fractured; ▼ granite, ground surface; ▽ limestone, gabbro, dunite; △ granite, ground surface; ○ Weber sandstone, faulted; ● Weber sandstone, saw cut; ■ granodiorite; ◇ gneiss and mylonite; ▫ plaster in joint of quartz monzonite; ◆ quartz monzonite joints; × Westerly granite, chlorite, serpentinite, illite, kaolinite, halloysite, montmorillonite, vermiculite; + granite; ⋄ kaolinite, halloysite, illite, montmorillonite, vermiculite.

Suppose the pore pressure is hydrostatic and take $\rho = 2.7$ gm/cm^2.

Then $\lambda = 1/2.7 = 0.37$

$$S_{ft} = (.85)(.63)(2.7) \cdot 10^3 \cdot 10^5$$

$$\boxed{S_{ft} = 150 \text{ bars per km depth}}$$

At a depth of 10 km the frictional strength is 1.5 kbars, at least an order of magnitude larger than the seismologically inferred stress drops. If Byerlee's law is applicable to the larger-scale field situation, it becomes very difficult to understand the remarkable constancy of $\Delta\sigma$. Why, if $\Delta\sigma$ is a very small fraction of the stress acting on the fault, should it be so constant for such a large range of earthquake sizes? If, on the other hand, the measured stress drops are an indication of the true strength of the fault zone, then the constancy of $\Delta\sigma$ becomes easier to understand.

A model which is increasingly being considered as possibly providing a

resolution of these difficulties is the asperity model.

Close observation has revealed that most, if not all, large 'quakes are complex multiple shocks consisting of a number of smaller events. This suggests that the distribution of $\Delta\sigma$ on the fault plane may actually be very heterogeneous so that each constituent event of a multiple shock corresponds to a high-stress asperity or region on the fault plane. Suppose:

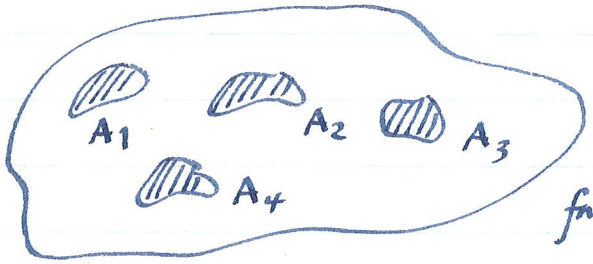

total fault area A

The stress everywhere except on the asperities is quite, low near zero. Only the strength of the asperities is preventing rupture. The stress drop measured using smooth $\Delta\sigma$ formulae as above will be related to the stress drop on asperity $\Delta\sigma_{asp}$ by

$$\Delta\sigma_{asp} = \frac{A}{\sum A_i}\,\Delta\sigma$$

The actual stress drop on the asperities may thus be much nearer the laboratory frictional strengths, in the approximate ratio $A/\Sigma A_i$.

Such models do not solve all the problems, of course. One must still ask why the stresses on the fault between the asperities are so low. It is possible that Byerlee's law is not immediately applicable to the gouge zone, or perhaps that fluid pressures are very high ($\lambda \approx 1$) so that the averaged frictional stresses on the fault plane are truly in the range 10 – 100 bars. Stresses on asperities may be 10 times larger, or more. There is also the question: if this is all true, why should the averaged stresses be so constant? This would seem to require constancy of $\Sigma A_i / A$.

The fact that stress and stress drop may however be very heterogeneous on the fault plane is however certainly an important realization.

The alternative to the low stress model is the high stress model, supported by some. This maintains that σ's on the fault are on the order of S_f, that $\Delta\sigma$ is a small fraction. Problems with this include absence of a heat flow anomaly on San Andreas (although this too is problematical), disagreement with plate tectonic driving force modelling.